DRAG REDUCTION OF SPORT UTILITY VEHICLE USING VORTEX GENERATORS

Yuri Antonio Sevilla
B.S., University of California, Davis, 2005

THESIS

Submitted in partial satisfaction of
the requirements for the degree of

MASTER OF SCIENCE

in

MECHANICAL ENGINEERING

at

CALIFORNIA STATE UNIVERSITY, SACRAMENTO

SUMMER
2012

DRAG REDUCTION OF SPORT UTILITY VEHICLE USING VORTEX GENERATORS

A Thesis

by

Yuri Antonio Sevilla

Approved by:

_____, Committee Chair
Dr. Dongmei Zhou

_____, Second Reader
Dr. Timothy Marbauch

_____
Date

Student: Yuri Antonio Sevilla

I certify that this student has met the requirements for format contained in the University format manual, and that this thesis is suitable for shelving in the Library and credit is to be awarded for the thesis.

_____, Department Chair _____
Dr. Susan Holl Date

Department of Mechanical Engineering

Abstract

of

DRAG REDUCTION OF SPORT UTILITY VEHICLE USING VORTEX GENERATORS

by

Yuri Antonio Sevilla

Road vehicles such as passenger cars, trucks and SUVs are categorized as bluff bodies. As a vehicle moves forward, the motion of the air around it produces pressure gradients, which vary across the entire body surface. This in turn helps to develop a turbulent wake region behind it, which works against the vehicle's forward motion. As a result, the engine has to work harder, thus increasing fuel consumption.

The purpose of this thesis is to present development, design and optimization of drag reducing devices for SUVs by examining the SUVs aerodymanic properties. Simulations using commercial software such as Solidworks, Ansys Workbench, Design Modeler, Mesh Editor and Fluent were performed to study the aerodynamic behavior behind the SUV. The Ahmed Reference Model (ARM) was selected as a benchmark test. Computational fluid dynamics (CFD) simulations for three SUV models were performed and their performance was analyzed to determine which design yields the best drag reduction results. The three CFD models consist of one basic SUV model without any drag reducing devices. The second one uses a bump-shaped vortex generator (VG) design and the third one uses a delta wing VG design. Out of the two VG designs, it was determined that the bump-shaped design yielded the best drag reduction results for the

SUV model. The next step was to experiment with the VG height to determine the optimum height for the SUV model. Results demonstrate that a bump-shaped VG with a height of 25 mm yields the lowest C_D.

_____, Committee Chair
Dr. Dongmei Zhou

_____
Date

ACKNOWLEDGMENTS

I would like to express my sincerest thanks to Dr. Dongmei Zhou for her guidance and support in the completion of my thesis. I would also like to thank Zerguy Maazouddin for his valuable advice and assistance. My thesis would have never been completed without them. Finally, I would like to thank the Mechanical Engineering Faculty for their encouragement, leadership, and help in the completion of my B.S. and M.S. degrees. Thank you for spreading the wealth of knowledge.

Yuri Antonio Sevilla
B.S. Mechanical Engineering
Spring 2005

TABLE OF CONTENTS

Page

Acknowledgments vi
List of Tables ix
List of Figures x
Chapter
1. MOTIVATION FOR PRESENT WORK 1
1.1 Introduction 1
1.2 Previous Work on Vortex Generators 2
1.2.1 Application of VGs on Airplanes 2
1.2.2 VG Application on a Sedan 3
1.2.3 VG Application on a Blunt Body 5
1.3 Outline for Present Work on Vortex Generators 9
2. VEHICLE AERODYNAMICS 11
2.1 Introduction 11
2.2 Automobile Aerodynamics 11
2.3 Flow Behavior Around Vehicles 14
2.4 Boundary Layer and Separation of Flow 17
2.5 Aerodynamic Forces Acting on Vehicle 20
3. SUV MODEL VALIDATION 25
3.1 Introduction 25
3.2 SUV Benchmark Parameters 26
3.2.1 Wind Tunnel Setup 26
3.2.2 Generic SUV Model Specifications 27
3.2.3 Test Results 29
3.3 Preparation for Benchmark Evaluation 32
3.3.1 SUV Benchmark Preparation 33
3.3.2 Mesh Setup 34
3.3.3 Fluent Solver Parameters 35
3.3.4 Results 37

3.4 Conclusion 41
4. EFFECT OF VORTEX GENERATORS ON SUV MODEL..... 42
4.1 Introduction to Vortex Generators 42
4.2 Bump-Shaped Vortex Generators on SUV Model 43
4.3 Wedge-Shaped Vortex Generators on SUV Model 45
4.4 Wind Tunnel and Vehicle Orientation 46
4.5 Mesh and Solver Settings 47
4.6 Results 49
4.6.1 Bump-Shaped VS Wedge-Shaped VG Results 49
4.6.2 Effect of VG Height on Drag 52
4.6.3 Effect of Reynolds Number on Drag 57
5. CONCLUSION AND FUTURE WORK 60
5.1 Summary 60
5.2 Future Work 61
References…..... 62

LIST OF TABLES

Page

1. Table 3.1 Solver settings……..…….…….…….... 36

2. Table 3.2 Viscous model settings…….…….…….…..... 36

3. Table 3.3 Boundary conditions and fluid properties…….……..….…..... 37

4. Table 3.4 Solution controls and residuals…….…….…..... 37

5. Table 4.1 Mesh quality results for the SUV models……..…...….…..... 48

6. Table 4.2 Drag results from simulations..……..…..….…..... 52

LIST OF FIGURES

Page

1. Figure 1.1 Location of VGs on aircraft wing [13]…..……...…...… 2

2. Figure 1.2 Location of VGs on Mitsubishi Lancer Evolution VIII [5]……..… 4

3. Figure 1.3 Results of height change on delta wing VG [5]…….……....… 4

4. Figure 1.4 Blunt body with VGs behind shoulder of boat-tail [11]…….....… 6

5. Figure 1.5 VGs redirecting airflow [11]…….……...……...… 7

6. Figure 1.6 Airflow without VGs [11]…..……...……...… 8

7. Figure 1.7 Effect of VGs on drag coefficient [11]…..……..……...… 9

8. Figure 2.1 Energy loss in a vehicle [16]…..…….……...…….… 12

9. Figure 2.2 Shape changes that help to reduce drag on SUV [3]……..…..... 13

10. Figure 2.3 Streamlines around a stationary vehicle [14]…….....……..……..….. 14

11. Figure 2.4 Pressure distribution on a vehicle [1]….……...……..….. 16

12. Figure 2.5 Boundary layer development [2]…….……..……...….. 17

13. Figure 2.6 Flow separation point caused by adversed pressure gradient [2]…... 19

14. Figure 2.7 Aerodynamic forces and moments acting on a vehicle [1]..……..... 24

15. Figure 3.1 Wind tunnel test section showing SUV model [4]…….……..... 26

16. Figure 3.2 Side view and rear view of the SUV model [4]…….. 28

17. Figure 3.3 Mean pressure coefficient along the symmetry plane [4]…..…...….. 30

18. Figure 3.4 downstream velocity profiles in the horizontal plane of wake [4]….. 32

19. Figure 3.5 Basic SUV geometry ……..…….…….…… 34

20. Figure 3.6 SUV orientation in relation to the wind tunnel ……..... 35

21. Figure 3.7 Meshing: Patch-conforming method with inflation layer on roof ….. 36

22. Figure 3.8 Simulated results of Cp plot over cab and underbody areas ……..... 39

23. Figure 3.9 Benchmark Cp plot for the cab and bottom sections of the SUV [4]...40

24. Figure 3.10 Comparison velocity magnitude streamlines [4]……..……..... 40

25. Figure 4.1 Mitsubishi Evolution with VGs [6]..…….. 43

26. Figure 4.2 Bump-shaped VG design with dimensions ……....…..…… 44

27. Figure 4.3 Location of bump-shaped VGs on SUV model ……..…….....…..… 44

28. Figure 4.4 Wedge-shaped VG design ……...……...… 45

29. Figure 4.5 Location of wedge-shaped VGs on SUV model ……..... 46

30. Figure 4.6 Wind tunnel and SUV orientation ……...…...…....…….. 47

31. Figure 4.7 Patch-conforming meshing method near bump-shaped VGs .....….. 48

32. Figure 4.8 Patch-conforming meshing method near the wedge-shaped VGs….... 48

33. Figure 4.9 Pressure contours from SUV model with no VGs……..…...…….. 50

34. Figure 4.10 Pressure contours from SUV model with bump-shaped VGs.…..... 51

35. Figure 4.11 Pressure contours from SUV model with wedge-shaped VGs …… 51

36. Figure 4.12 Pressure contours in wake region for varying VG heights ……..… 54

37. Figure 4.13 Pressure contours on roof of SUV for varying VG heights..... 55

38. Figure 4.14 Velocity vectors on roof for varying VG heights ……....….... 56

39. Figure 4.15 C_D for different VG heights ...…….……..… 57

40. Figure 4.16 Flow around a vehicle ……..…… 58

41. Figure 4.17 Pressure contours in wake region at different velocities ……..… 59

42. Figure 4.18 Pressure contours on roof of SUV at different velocities..... 59

43. Figure 4.19 Velocity magnitude in wake region at different velocities…..…….. 59

Chapter 1

MOTIVATION FOR PRESENT WORK

1.1 INTRODUCTION

The purpose of this thesis is to present the development and design of drag reducing devices for an SUV, by studying the vehicle's aerodynamics. Aerodynamics plays an important role in vehicle design. With the ever increasing prices of oil and the countries movement towards reducing its dependence on foreign oil, it is the vested interest of engineers to find and develop methods to increase fuel economy. By applying the principles of aerodynamics, it is possible to reduce the coefficient of drag (C_D) of a vehicle and thus contribute to its fuel efficiency. Most of the research on the benefits of VGs has been conducted in the field of aviation. Some research has also proven that VGs can produce measurable improvements in drag reduction on vehicles. In addition to having the potential to reduce the coefficient of drag C_D on a vehicle, there are other benefits to using VGs on a passenger vehicle. For example, they can help reduce soiling of the rear window. Also, unlike other drag reduction devices currently in the market such as spoilers, wings and front splitters, VGs have a less prominent appearance on vehicles, while still providing drag reduction benefits. In addition, they are relatively easy to install and remove without leaving any permanent marks on the mounting surface, which can potentially affect the resale value of a vehicle. Finally, they tend to be more cost effective than the alternatives mentioned above.

1.2 PREVIOUS WORK ON VORTEX GENERATORS

1.2.1 APPLICATION OF VGs ON AIRPLANES

As was previously mentioned, most of the research on VGs has concentrated on the field of aviation, which is where the concept originated from. In an aircraft, VGs are typically installed in the wing area, where they promote the adherence of air to the wing's surface as seen on ***Figure 1.1***. As air normally flows over the wing of an aircraft in flight, it sticks to the surface of the wing. This adherence to the wing's surface produces lift. If the airflow loses its adherence and separates from the wing, the aircraft's performance can suffer in the form of increased drag, loss of lift and higher fuel consumption. By preventing the air from detaching from the wing's surface, drag is reduced and thus fuel consumption is minimized. This results in an increase in the aircraft's maximum cruise speed, extending its operational range and improving controllability [13].

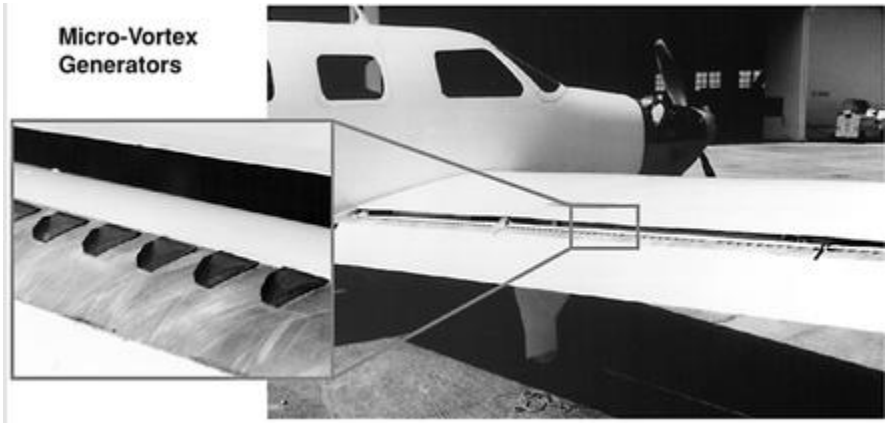

Figure 1.1 Location of VGs on aircraft wing [13].

1.2.2 VG APPLICATION ON A SEDAN

Previous research conducted at Mitsubishi Motors by Koike, Nagayoshi and Hamamoto shows that VGs can contribute to drag reduction on sedans. A Mitsubishi Lancer Evolution VIII was tested on a full scale wind tunnel with a main flow velocity of 50 m/s [5]. The optimum height of VGs is estimated to be the same as that of the boundary layer thickness of the vehicle. However, it's important to note that although VGs can reduce drag, they can also increase drag if the height goes beyond a certain point. In term of the position, an area just before the point of flow separation on the roof was considered ideal as seen on ***Figure 1.2***. After testing heights of *15 mm, 20 mm and 25 mm*, it was determined that a height of *20-25 mm* yielded the best results as seen on ***Figure 1.3***.

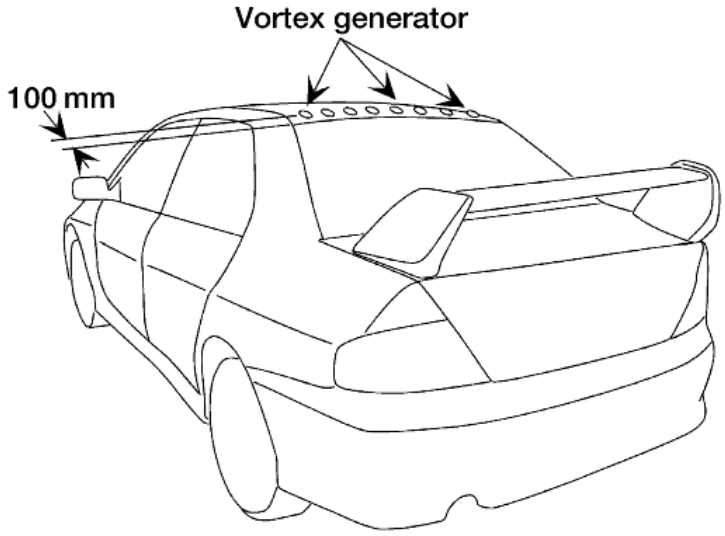

Figure 1.2 Location of VGs on Mitsubishi Lancer Evolution VIII [5].

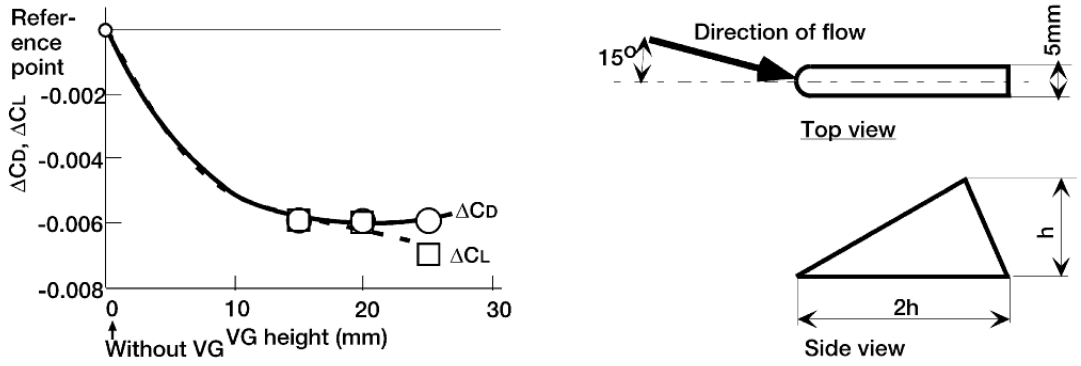

Figure 1.3 Results of height change on delta wing VG [5].

Delta wing VGs were found to be more tolerant of height changes than bump-shaped VGs. After experimenting with the height, angle position, and total number of VGs, it was found that using bump-shaped VGs resulted in a drag reduction C_D of *0.003*,

while the delta wing VGs provided a drag reduction C_D of *0.006*. This can be attributed to the fact that delta wing VGs have a smaller cross-sectional area than the bump-shaped VGs, hence the reason why they create less drag.

1.2.3 VG APPLICATION ON A BLUNT BODY

Gustavsson and Melin at KTH conducted experiments to determine the benefit of VGs when applied to blunt bodies. Simulations of a blunt body were performed in a wind-tunnel. Due to limitations set up by the Swedish National Road Administration (SNRA), which indicate that no part of the vehicle may extend beyond the vehicle's perimeter, the decision was made to place the VGs just behind the shoulder of the body, as seen on **Figure 1.4** . The dimensions of the main body consisted of *L = 0.95 m, W = 0.50 m and H = 0.30 m*, with a boat-tail angle of *40°*. The objective of the first wind tunnel test was to determine the effectiveness of VGs at redirecting airflow.

Figure 1.4 Blunt body with VGs placed behind shoulder of boat-tail.

The test was found to be successful and confirmed that VGs can be used to redirect airflow in the back to the body. ***Figure 1.5*** and ***Figure 1.6*** show the airflow behavior with and without VGs respectively. While the first wind tunnel test proved that VGs can be used to redirect airflow, it still did not establish the effect of VGs on drag. Therefore, another wind tunnel test was performed. This time VGs were placed before the shoulder. Additionally, a combination of boat tail angles of *20°, 40°, 60° and 90°* were also used. Different VG heights and lengths were also tested. ***Figure 1.7*** shows the results from the experiment. The results show that the lowest drag configuration was Cd = 0.4540 and was obtained with a boat tail angle of *40°* and no VGs. Gustavsson and Melin conclude that based on the their initial findings, the most beneficial approach in reducing bluff body drag is to equip the vehicle with a 50° boat tail and leave out the VGs. However,

they also point out that the tests performed so far are not to be considered conclusive and that more research needs to be performed.

Figure 1.5 VGs redirecting airflow.

Figure 1.6 Airflow without VGs.

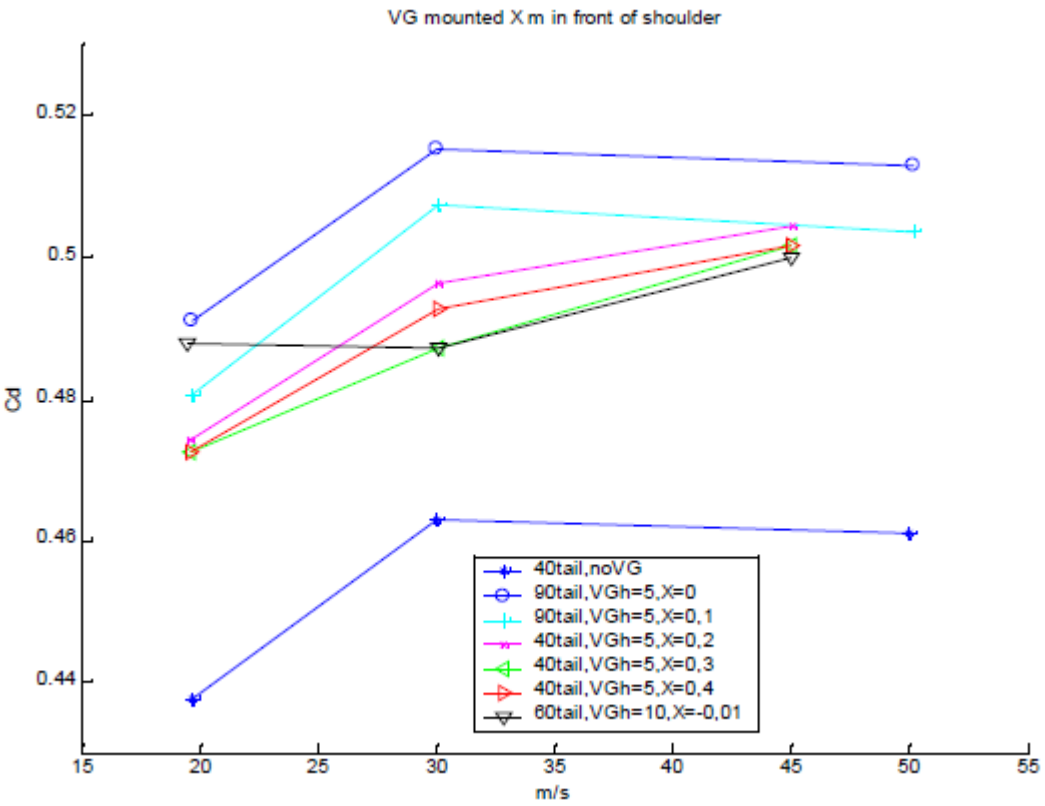

Figure 1.7 Effect of VGs on drag coefficient.

1.3 OUTLINE FOR PRESENT WORK ON VORTEX GENERATORS

First, a background on vehicle aerodynamics will be covered, including explanation of the concepts and formulas involved. Next, the procedure for building a basic model, including the SUV and wind tunnel, along with dimensions and simulation parameters, will be developed. The basic model will then be compared with a reputable benchmark to confirm validity of the simulation setup and corresponding results. Once the basic simulation model is benchmarked, it will then be modified to include the

external drag reduction devices. Two different VG designs will be studied, which include a delta wing design and bump-shaped design. Once the basic VG design is established, the next step will be to experiment with difference VG heights in order to determine the ideal height for the SUV model. CFD simulations will be performed on the modified models to examine the results and determine the changes. Once the data for all simulations has been acquired the results will be summarized. Finally, a discussion of future work to be performed will be covered.

Chapter 2

VEHICLE AERODYNAMICS

2.1 INTRODUCTION

Aerodynamics is the study of a solid body moving through the atmosphere and the interaction, which takes place between the body surfaces and the surrounding air with varying relative speeds and wind direction [2]. Some of the properties that are of particular interest in the field of aerodynamics are mass, pressure, density, velocity and temperature. The use of those properties, in conjunction with mathematical analysis, empirical approximation and wind tunnel testing, allows an engineer to come up with results that can be applied to future vehicles that will progressively become more efficient. Aerodynamics, as it applies to vehicles, is basically divided into two categories, internal and external flow. Some examples of internal flow on vehicles would be heating and air conditioning system, as well as the flow around the engine compartment. While, external flow relates to the air movement around the external surfaces of the vehicle's body.

2.2 VEHICLE AERODYNAMICS

The constant need for better fuel economy, greater vehicle performance and improved stability, has prompted vehicle manufacturers to investigate the nature of air resistance or drag for different body shapes under various operation conditions. Energy efficiency of vehicles can be improved in three ways. By 1) reducing the total structural

mass, 2) using an engine with a higher thermally efficiency or 3) altering the exterior body shape to reduce the aerodynamic drag. The US department of energy [8] estimates that only 12.6% of the fuel being consumed is actually used to propel the vehicle forward as shown in ***Figure 2.1***. Furthermore, out of that 12.6% of remaining energy, an additional 2.6% is used to overcome aerodynamic drag. This is the reason why optimizing vehicle aerodynamics is essential to the improvement of fuel efficiency, especially at higher speeds.

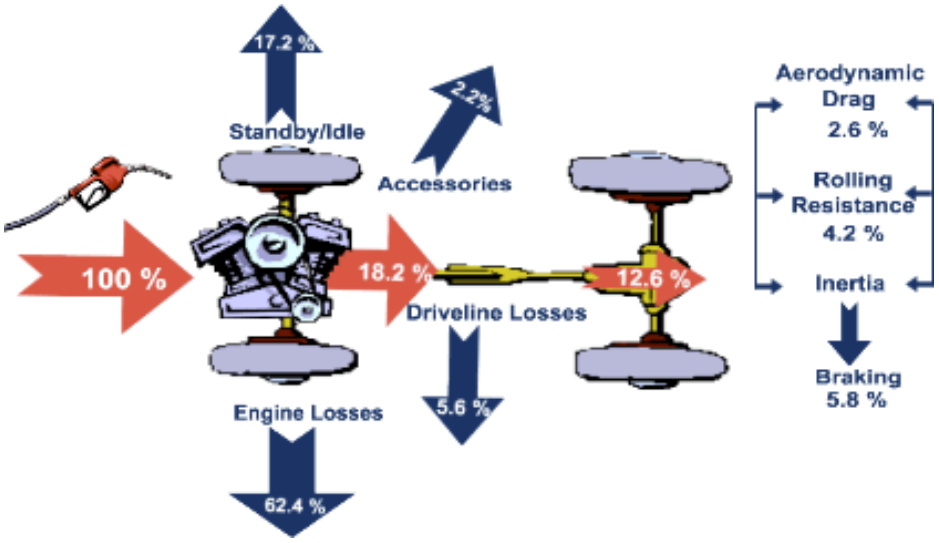

Figure 2.1 Energy loss in a vehicle [16].

When it comes to vehicle aerodynamics, the focus is aerodynamic drag. In particular, the non-dimensional number known as the drag coefficient (C_D). Aerodynamic drag is usually insignificant at low speeds but the magnitude of air resistance becomes considerable with rising speed.

There is no denying the fact that aerodynamics plays a significant role in vehicle design. However, a designer has to keep in mind that the overall shape and detail of a vehicle is determined by many other factors. Factors such as function, safety, regulations, economy and aesthetics all have to be carefully implemented in the design to achieve a proper balance. Existing solutions [3] to reduce aerodynamic drag include: using external attachments, larger leading edge radius, hood inclination and spoiler at the front, inclining the windshield, arching the roof, budging out the sides and smoothing the underbody surface as seen on ***Figure 2.2***.

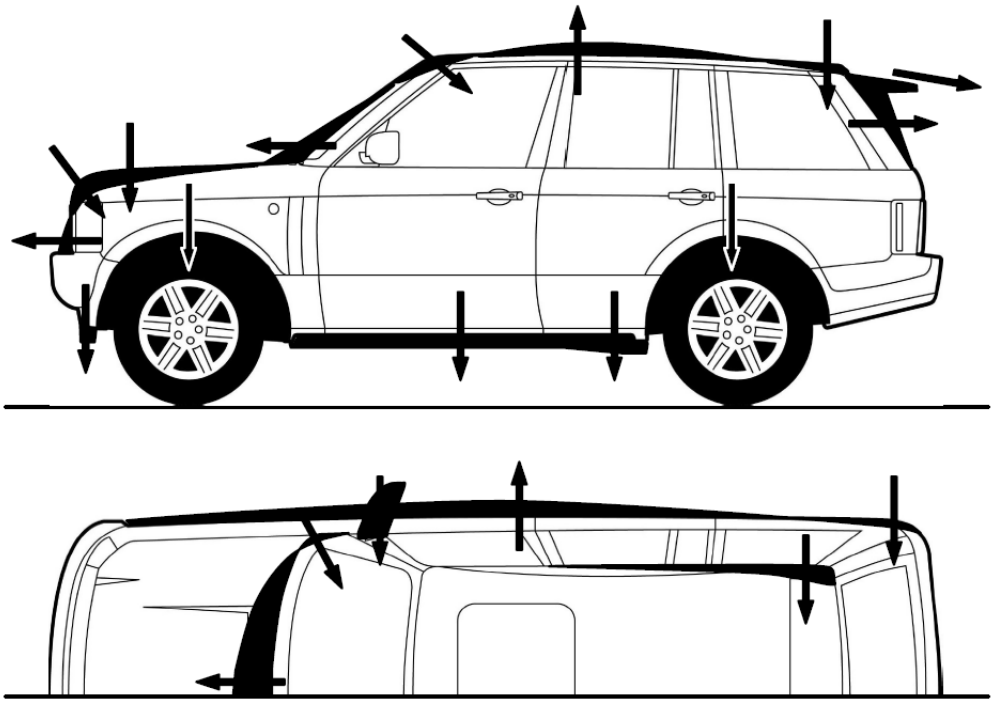

Figure 2.2 Shape changes that help to reduce Drag on SUV [3].

This thesis will focus on the implementation of external devices that will help reduce the aerodynamic drag on SUVs, while still maintaining a subtle an aesthetically pleasing shape.

2.3 FLOW BEHAVIOR AROUND VEHICLES

External flow past objects encompass an extremely wide variety of fluid mechanics phenomena and the characteristic of the flow fields is a function of shape of the body. If we were to visualize a stationary vehicle and air moving, much like a wind tunnel, we would see steady streamlines ahead of the vehicle as seen on ***Figure 2.3***. At a distance from the vehicle, the static pressure is simply the ambient pressure (P_{atm}). However, as the flow approaches the vehicle, the steady streamlines begin to split, some going above the vehicle while others go below.

Figure 2.3 Streamlines around a stationary vehicle [14].

Consider what happens to the streamlines that go above the vehicle. As they first begin to make their way over the hood, the curvature is concave upwards. At a distance far above the streamlines are straight and the static pressure is the same as the atmosphere. Therefore, in order for the streamlines to curve upward, the static pressure in that region must be higher than ambient. Consequently, the velocity in this region must be slower in order to obey Bernoulli's equation, which is expresses as:

$$P_{total} = P_{static} + P_{dynamic} \tag{2.1a}$$

$$P_t = P_s + \frac{1}{2}\rho V^2 \tag{2.1b}$$

where:

$\rho = Density\ of\ Air$

$V = Velocity\ of\ Air$

As the flow turns to follow the hood, the streamline curvature becomes concave downward. The pressure goes below ambient to bend the flow and the velocity increases as seen on ***Figure 2.4.***

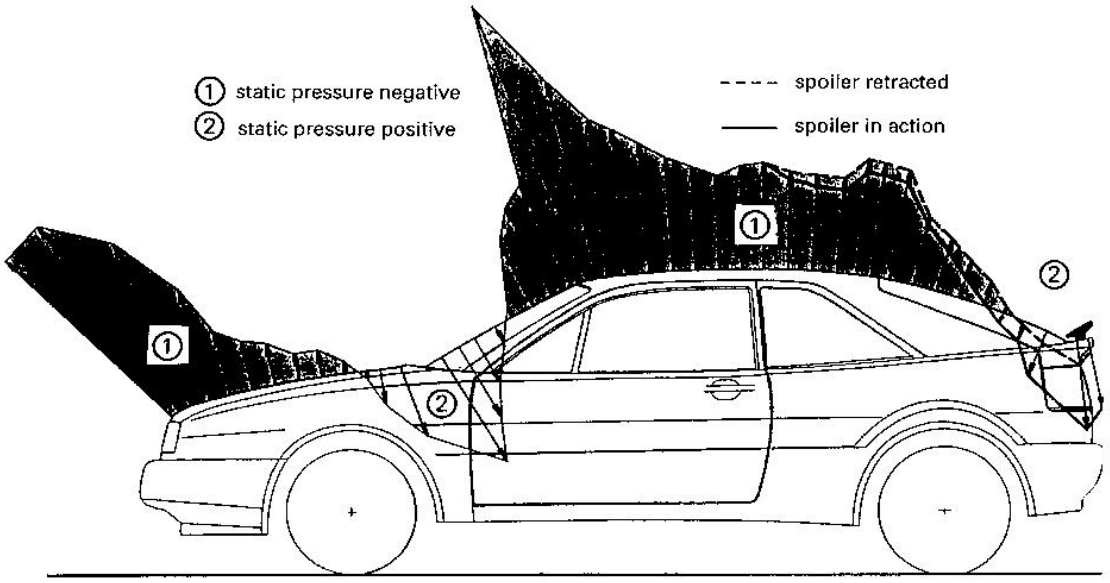

Figure 2.4 Pressure distribution on a vehicle [1].

When the streamlines approach the windshield, once again the pressure goes up, while velocity goes down, to create that concave upward curvature on the streamlines. Once they reach the leading edge of the roof, pressure drops and velocity increases, as the streamlines follow the flat surface of the roof. Now, if the there was no air friction, the streamlines would just continue to follow the roof line and back down the back of the vehicle, in which case the pressure forces on the rear of the vehicle would balance the ones on the front and no drag would be created.

However, drag is in fact produced and it's due in part to the friction that occurs between the air and the surface of the vehicle, as well as the way the friction alters the main flow towards the rear of the vehicle.

2.4 BOUNDARY LAYER AND SEPARATION OF FLOW

Before reaching the vehicle's body, the air has a constant velocity, which is considered well-behaved and laminar. However, once it contacts the vehicle's surface the air velocity drops to zero due to friction on the surface and a velocity profile develops. Within this small section, the velocity is lower than the main flow. This region of lower velocity is known as the boundary layer. In this relatively small region adjacent to the vehicle, the effect of viscosity must be taken in to account. The boundary layer essentially starts at zero thickness and develops as it moves towards the back of the vehicle. Initially, the flow in this area is laminar, but eventually it becomes turbulent as seen on ***Figure 2.5***.

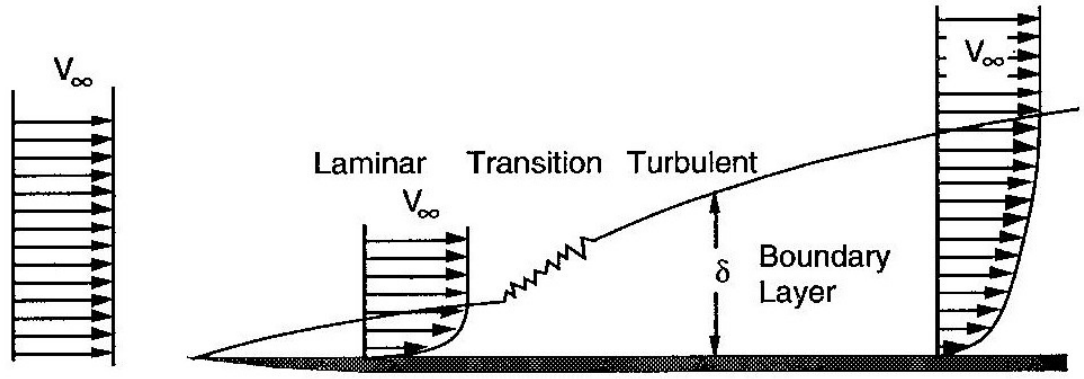

Figure 2.5 Boundary layer development [2].

The concept of a boundary layer was first introduced by Ludwig Prandtl in 1904. Outside this region the boundary layer is assumed to be inviscid or frictionless. Therefore, viscosity is neglected in the fluid regions outside this boundary layer since it does not have significant effect on the solution. In the design of the body shape, the boundary layer is given high attention to reduce drag. There are two reasons why designers consider the boundary layer as a major factor in aerodynamic drag. The first is that the boundary layer adds to the effective thickness of the body, through the displacement thickness, hence increasing the pressure drag. The second reason is that the shear forces at the surface of the vehicle causes skin friction drag.

During the flow over the surface of the vehicle, there is a point when the change in velocity comes to a stall and the fluid starts flowing in reverse direction. This phenomenon is called "adverse pressure gradient" and can be seen in ***Figure 2.6***. The point where the flow stops is known as the "separation point". At this point the main stream is no longer attached to the body. The pressure in this region drops below ambient and vortices begin to form, causing a very irregular flow in the region [5].

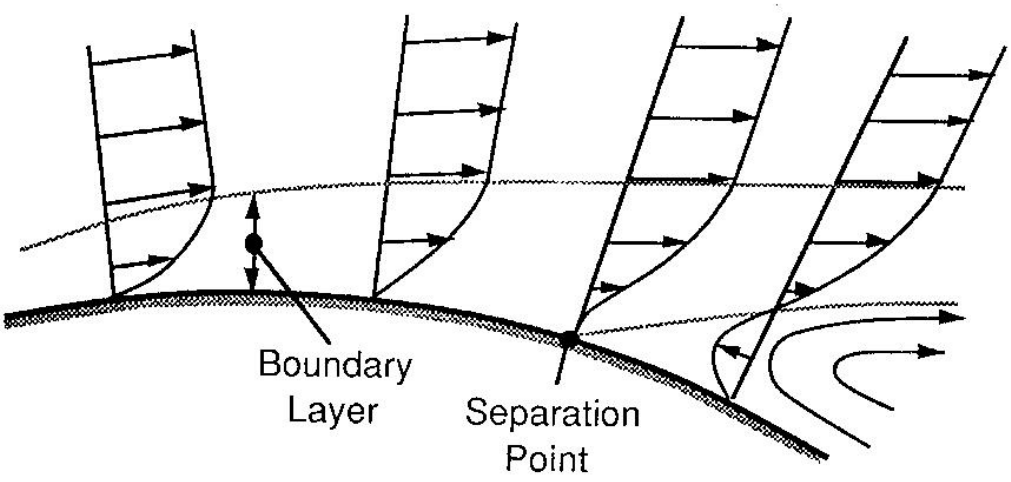

Figure 2.6 Flow separation point caused by adversed pressure gradient [2].

This is usually occurs in the rear section of the vehicle. The separation point is highly dependent on the pressure distribution which is imposed by the outer layer of the flow. The turbulent boundary layer can withstand much higher pressure without separating as compared to laminar flow. This separation phenomenon is what prevents the flow from proceeding down the back side of a vehicle. The pressure in the separation region is lower than the one in front of the vehicle and the difference in this pressure forces is responsible for "form drag". The drag forces that develop from viscous friction in the boundary layer on the surface of the vehicle are what causes "friction drag".

2.5 AERODYNAMIC FORCES ACTING ON VEHICLE

Aerodynamic forces acting on a vehicle are produced by the interaction of the airflow with the vehicle. The interaction of the airflow with the vehicle produces aerodynamic forces and moments: aerodynamic drag, aerodynamic lift, sideforce, rolling moment, pitching moment, and yawing moment. ***Figure 2.7*** shows the three aerodynamic forces and the three moments acting on the principal axes of a vehicle, where, *T(D)* is aerodynamic drag, *M* is the rolling moment, *Y* is the sideforce, *N* is the pitching moment, *L* is aerodynamic lift, and *R* is the yawing moment. The origin for the measurement of the three aerodynamic forces and moments is in the ground plane at the middle of the wheelbase and track position. The sideforce comes from taking into account random airflow, and if the airflow is only assumed normal to the vehicle then that will define aerodynamic drag. ***Figure 2.7*** also shows a vector force diagram of the airflow approaching the vehicle. V_∞ is the velocity of random wind or airflow approaching the vehicle with a yawing angle β. $-V_F$ is the velocity of the random airflow parallel to the vehicle and V_S is the airflow velocity that is normal to the vehicle. The vector sum of V_S and $-V_F$ yields V_∞.

Aerodynamic drag is the most important aerodynamic force because it accounts for 65% of the total force acting on the vehicle's body. It is the main contributor because of the low-pressure turbulent wake region that forms at the base of the vehicle. The following equation is used to calculate aerodynamic drag:

$$D = \frac{1}{2}\rho V^2 C_D A \tag{2.2}$$

where:

C_D = Aerodynamic Drag Coefficient

V = Velocity of Vehicle

A = Frontal Area of Vehicle

ρ = Air Density

The $\frac{1}{2}\rho V^2$ term represents the dynamic pressure. The aerodynamic drag coefficient is determined experimentally form the wind tunnel tests and standard conditions of $15^{\circ}C$ and atmospheric pressure are assumed for the air density.

Aerodynamic lift is mainly the pressure difference on the top and bottom of a vehicle. Aerodynamic lift has a strong influence on driving stability and it is very important not to negatively affect it so that the vehicle remains stable. If aerodynamic lift increases too much then it will cause the wheels on a vehicle to have less attraction force with the road, and this will cause the vehicle to become very unstable and risk rollover. The following equation for aerodynamic lift is expressed as:

$$L = \frac{1}{2}\,\rho V^2 C_L A \tag{2.3}$$

where:

L_A = Lift Force

C_L = Lift Coefficient

A = Frontal Area of Vehicle

The sideforce is crosswind acting on the vehicle and under the steady state wind conditions the equation for sideforce calculation is expressed as:

$$Y = \frac{1}{2}\rho V^2 C_S A \tag{2.4}$$

where:

Y = Sideforce

V = Total Wind Velocity

C_S = Side Force Coefficient (Function of Relative Wind Angle)

A = Frontal Areal of Vehicle

The pitching moment, N, transfers weight between the front and rear axles and is represented by the following equation:

$$N = \frac{1}{2}\rho V^2 C_{PM} A L \tag{2.5}$$

where:

N = Pitching Moment

C_{PM} = Pitching Moment Coefficient

A = Frontal Area of Vehicle

L = Wheelbase

Crosswinds produce a sideforce on a vehicle that acts at the middle of the wheelbase, and when the crosswinds do not act at the middle of the wheelbase a yawing moment is produced. The yawing moment represented by the following equation:

$$R = \frac{1}{2}\rho V^2 C_{YM} A L \tag{2.6}$$

where:

R = Yawing Moment

C_{YM} = Yawing Moment Coefficient (Varies with Wind Direction)

A = Frontal Areal of Vehicle

L = Wheelbase

When the crosswind produces a sideforce at an elevated point on a vehicle, a rolling moment is produced and is represented by the following equation:

$$M = \frac{1}{2}\rho V^2 C_{RM} A L \tag{2.7}$$

where:

M = Rolling Moment

C_{RM} = Rolling Moment Coefficient (Varies with Wind Direction)

A = Frontal Area of Vehicle

L = Wheelbase

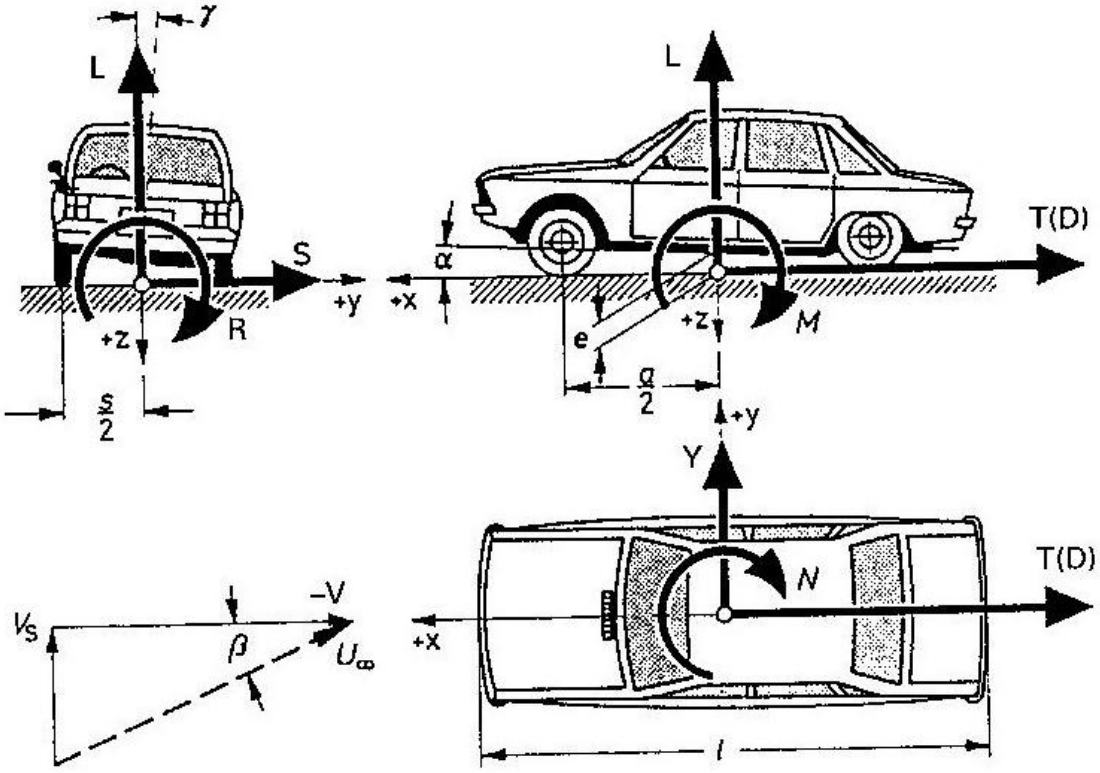

Figure 2.7 Aerodynamic forces and moments acting on a vehicle [1].

Chapter 3

SUV MODEL VALIDATION

3.1 INTRODUCTION

Before summiting a particular CFD model to rigorous testing procedures, it's generally recommended to first find a previously established benchmark. A benchmark is essentially a set of standards which can be used a point of reference in order to evaluate the level of quality of a given model. The objectives of benchmarking are 1) to determine what and where improvements are called for, 2) to analyze how other models achieve their high performance levels, and 3) to use this information to improve performance.

For the CFD model, the benchmarking process should yield guidelines for a specific class of problems. These guidelines will describe the initial parameters such as atmospheric conditions, boundary conditions, turbulence model and meshing strategy (clustering and growth rate) required to achieve a desired level of confidence and accuracy in the results. Once these guidelines have been found, they would then be applied to the new model, in order to determine the consistency and quality of the results.

For current benchmarking process, the generic SUV model will be simulated. The Generic SUV model was fabricated at Michigan University with assistance from General Motors. A wind tunnel test was performed on SUV model using advance PIV techniques. The results of this wind tunnel test are compared with the results of the numerical simulations using analytical solvers like Fluent.

3.2 SUV BENCHMARK PARAMETERS

3.2.1 WIND TUNNEL SETUP

The generic SUV model that was developed by Michigan University is a 1:12 scale model. The experiment was conducted in an open-return suction wind tunnel equipped with sided walls made of glass so that visual observation could be made while conducting the experiment [7]. The test section cross-section area is about 0.60 x 0.60 m^2. Within the tunnel there is a 2 meter long ground board, mounted 0.1 *m* below the top wall to simulate ground effects on the SUV flow as seen on ***Figure 3.1***.

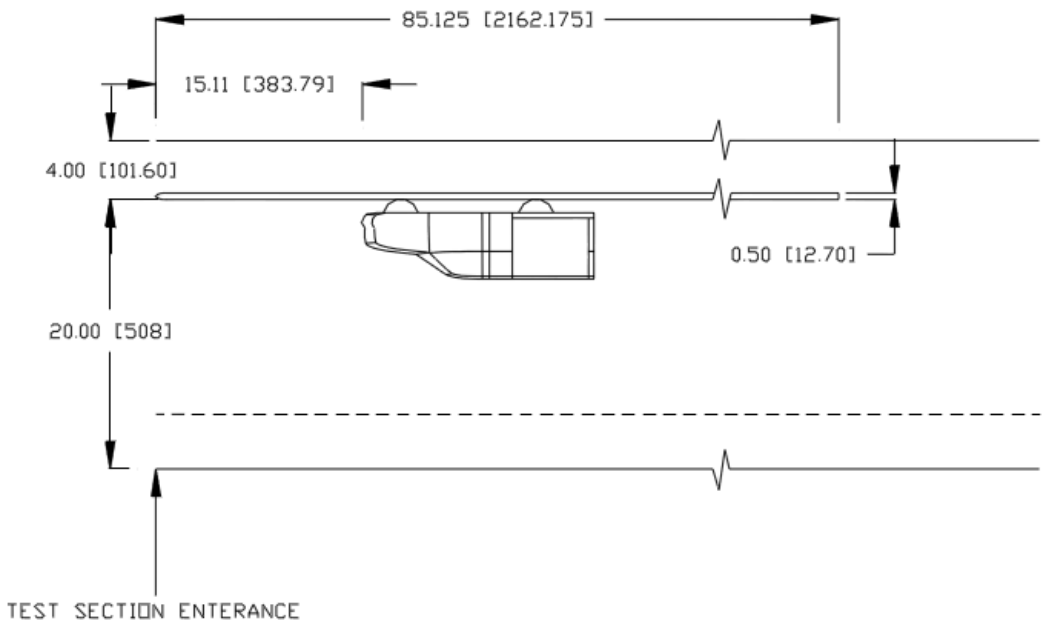

Figure 3.1 Wind tunnel test section showing SUV Model [4]

3.2.2 GENERIC SUV MODEL SPECIFICATIONS

Figure 3.2 shows that SUV model along with the detailed dimensions. The length of the model is *432 mm*, the width is *152 mm* and the height is *148 mm*. The maximum cross section is approximately *0.019* m^2, which yields a blockage area ratio of 5.2%. Furthermore, the origin of the coordinate system is right at the base of the front bumper. The x-axis is in the direction of incoming flow. The z-axis represents the vertical direction while the y-axis is perpendicular to the incoming flow. Additionally, the SUV model was fitted with a total of seventy pressure taps located along the symmetry plane as well as the base of the model. Unsteady pressure measurements were conducted at the central point of the base.

A quick inspection of this generic model shows the typical shape of an SUV. The front bumper, hood, windshield and roof consist of very smooth detailed shapes. In contrast, areas such as the underside, the rear and the wheels consist of very flat surfaces with very little detail. This is done to facilitate the mesh generation as well as the CFD analysis. The CAD model is defined in such a way that the most important aerodynamic characteristics of the SUV are maintained, thereby minimizing the use of heavy computational resources during the numerical analysis.

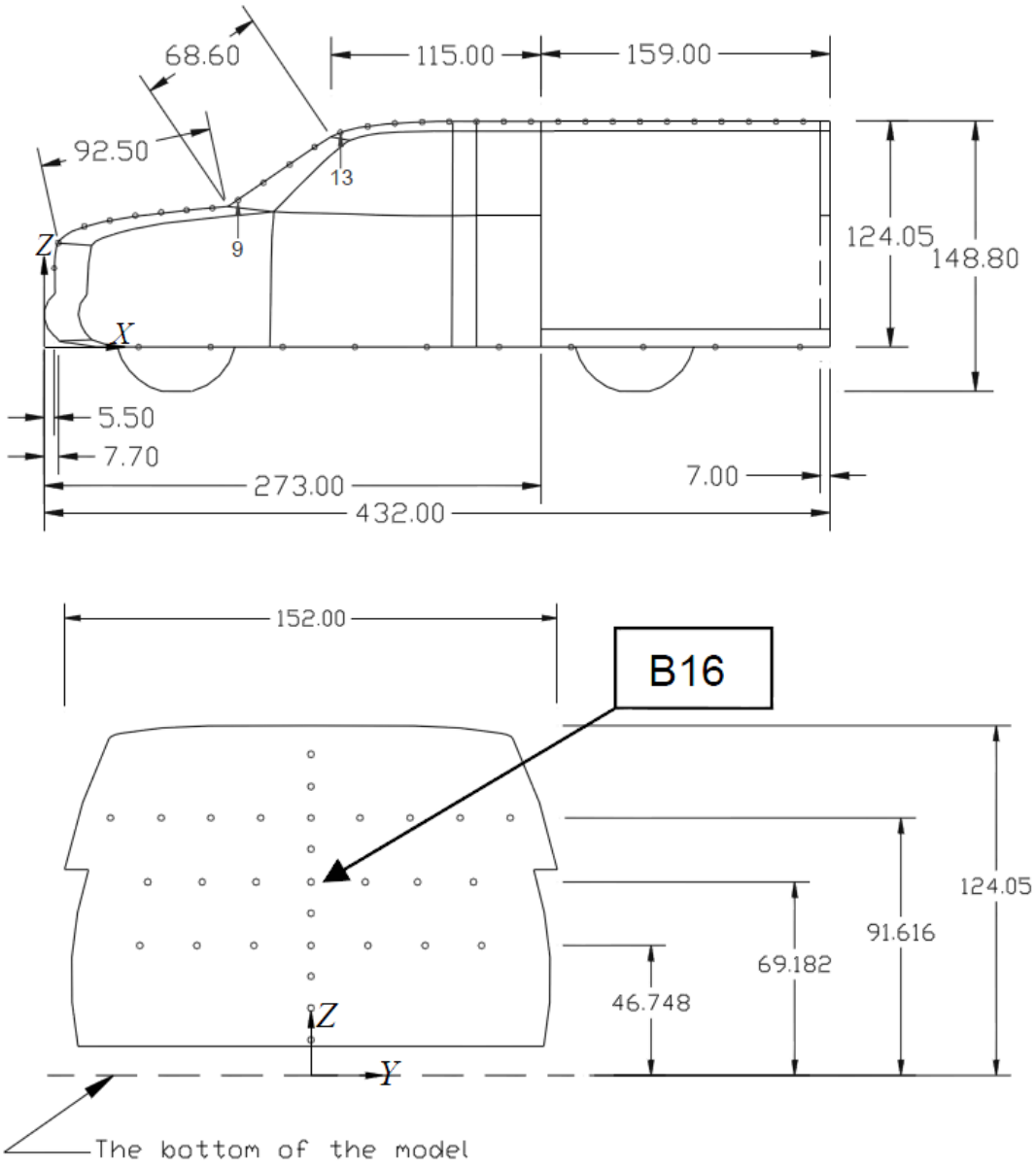

Figure 3.2 Side view and rear view of the SUV model [4]

3.2.3 TEST RESULTS

The mean pressure measurements were made at the symmetry plane, including the top and bottom surfaces of the SUV model. Additionally, several other pressure tabs were strategically placed at the base of the SUV. The test was conducted at a free stream velocity of 30 *m/s* which corresponds to a Reynolds Number (Re #) of 8×10^5, based on a model length of $L = 0.432\ m$. ***Figure 3.3*** reveals the mean pressure coefficient along the symmetry plane of the model. Two distinct curve plots are shown. The curve labeled "Cab" refers to the top surfaces of the SUV model, while the curve labeled "Bottom" corresponds to the underside. It's worth mentioning that there seems to be a typo in ***Figure 3.3*** as it shows a Reynolds Number value of 2.88×10^5 instead of the previously mentioned value of 8×10^5. This can be easily verified by plugging in the given velocity and characteristic length of the model into the Reynolds equation, which yields the expected value of 8×10^5.

In Aerodynamics, the pressure coefficient is a dimensionless number used to describe the relative pressure throughout a flow field. Every point in the flow field has a unique pressure coefficient C_P. This value is expressed in the following equation:

$$Cp = \frac{p - p_\infty}{\frac{1}{2}\rho_\infty V_\infty^2} \tag{3.1}$$

where:

p = Pressure at point of interest

p_∞ = Atmospheric pressure

ρ_∞ = Atmospheric fluid density

V_∞ = Free stream velocity

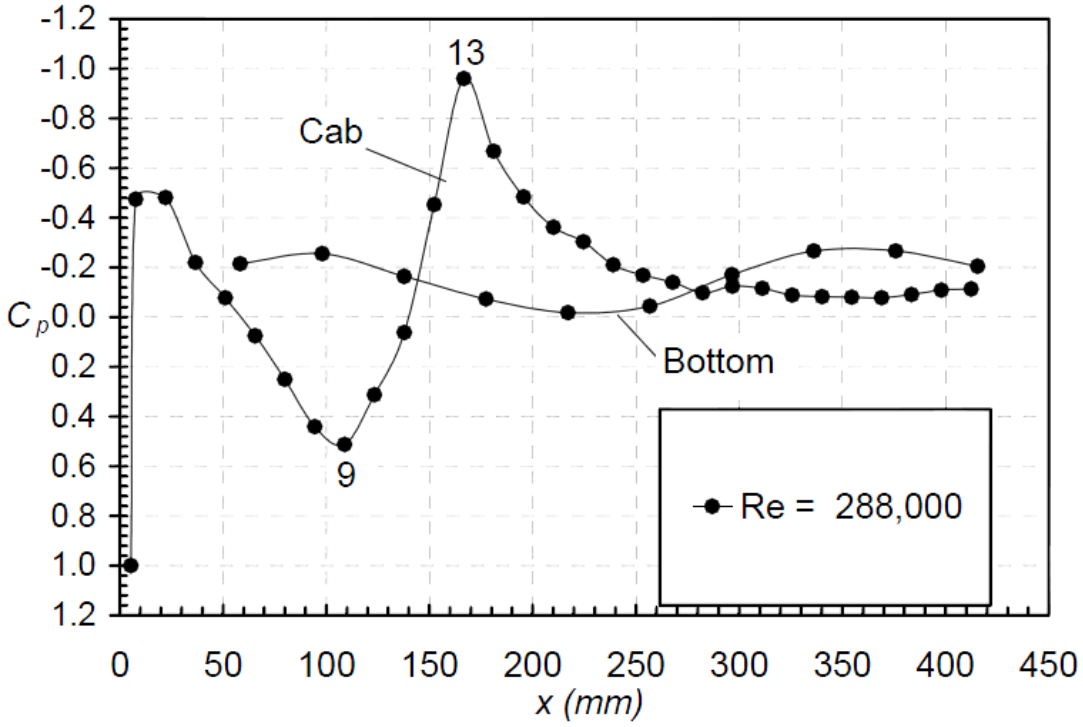

Figure 3.3 Mean pressure coefficient along the symmetry plane [4]

Note that on ***Figure 3.3***, the vertical axis is inverted. Negative values of the C_P are on top while the positive values are at the bottom of the graph. The results demonstrated in ***Figure 3.3*** can be interpreted as follows. When the free streamlines hit the front bumper of the SUV, the relative velocity goes to zero which is represented by the coefficient of pressure (C_P) value of 1.0 at this point. As the streamlines curve up, the static pressure increases while velocity decreases, resulting in a negative C_P value. This negative C_P quickly changes back to a positive value as the streamline reaches the leading

edge of the hood. Next, the pressure decreases and the flow velocity increases as the streamlines curve down to travel along the hood. The point labeled "9" is a critical, high pressure area, located at the bottom of the windshield. This high pressure is the ideal area to place the inlet for ventilation systems on a vehicle. As the streamlines reach the top edge of the windshield (point "13"), pressure once again decreases and velocity increases so the streamlines can travel parallel to the roof surface. Flow along the surface of the roof remains steady. However, as the streamlines make their way towards the rear edge of the roof, turbulence begins to form, causing separation of the air at the end of the roof.

Figure 3.4 shows the mean velocity profiles in the center horizontal plane of the wake located at 450 mm, 500 mm, 550 mm, 600 mm and 700 mm measured by the PIV method in the wake region of the SUV model at the horizontal plane. Although several forms of experimental data has been collected, only the pressure coefficient data at the symmetry plane will be used for the validation process. This is done to support the decision of using the symmetry plane in CFD analysis. The use of symmetry plane complies with the limited computational resources.

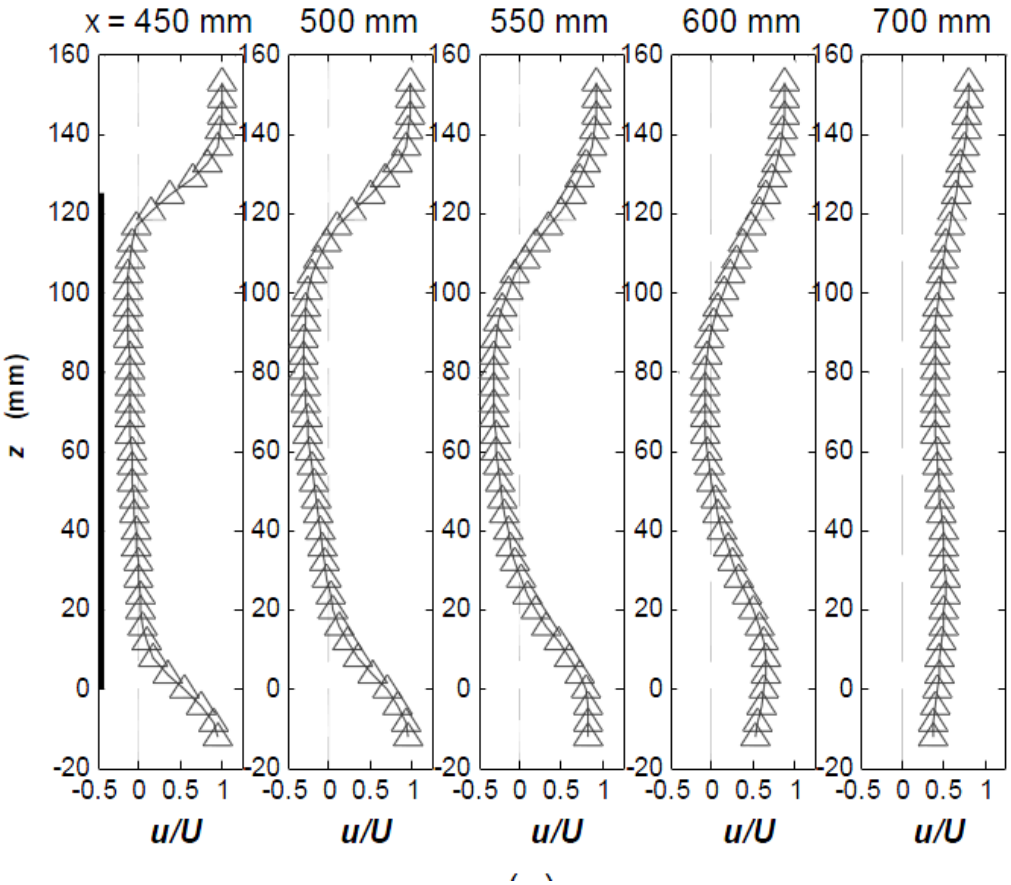

Figure 3.4 Downstream velocity profiles in the horizontal plane of wake [4]

3.3 PREPARATION FOR BENCHMARK EVALUATION

Now that a suitable benchmark test has been selected, the next step is to prepare the current SUV model for the numerical evaluations and compare the results and compare the results with the previously established benchmark. The software being used for this analysis consists of Solidworks®, Ansys® 13 software package which includes 1) Workbench, 2) Design Modeler, 3) Mesh Generator and 4) Fluent.

3.3.1 SUV BENCHMARK PREPARATION

Figure 3.5 shows the basic CAD model used to conduct wind tunnel experiments at the University of Michigan. The basic SUV geometry comes from Mr. Khalighi, who was involved in the wind tunnel experiments that were discussed in the previous section. The first step in the benchmark simulation was to create the wind tunnel around the SUV model Using Solidworks. Based on the dimensions defined in *section 2.2.1* the wind tunnel inlet is placed at two times the length of the SUV ahead of the SUV with the origin located at base of the front bumper. The pressure outlet is placed at five times the length of the SUV, just behind the rear of the SVU. ***Figure 2.6*** shows the location of the SUV in relation to the wind tunnel. The wind tunnel has a cross section of $0.60 \times 0.60\ m^2$. However, it's important to notice that the wind tunnel contains a ground plate that spans the entire length of the tunnel and is located *0.10 m* from the wind tunnel surface. Therefore, the cross sectional area of the test area is $0.60 \times 0.50\ m^2$. The inlet of the Wind tunnel in the simulation is given maximum velocity of *30 m/s*, while the outlet pressure is defined as zero.

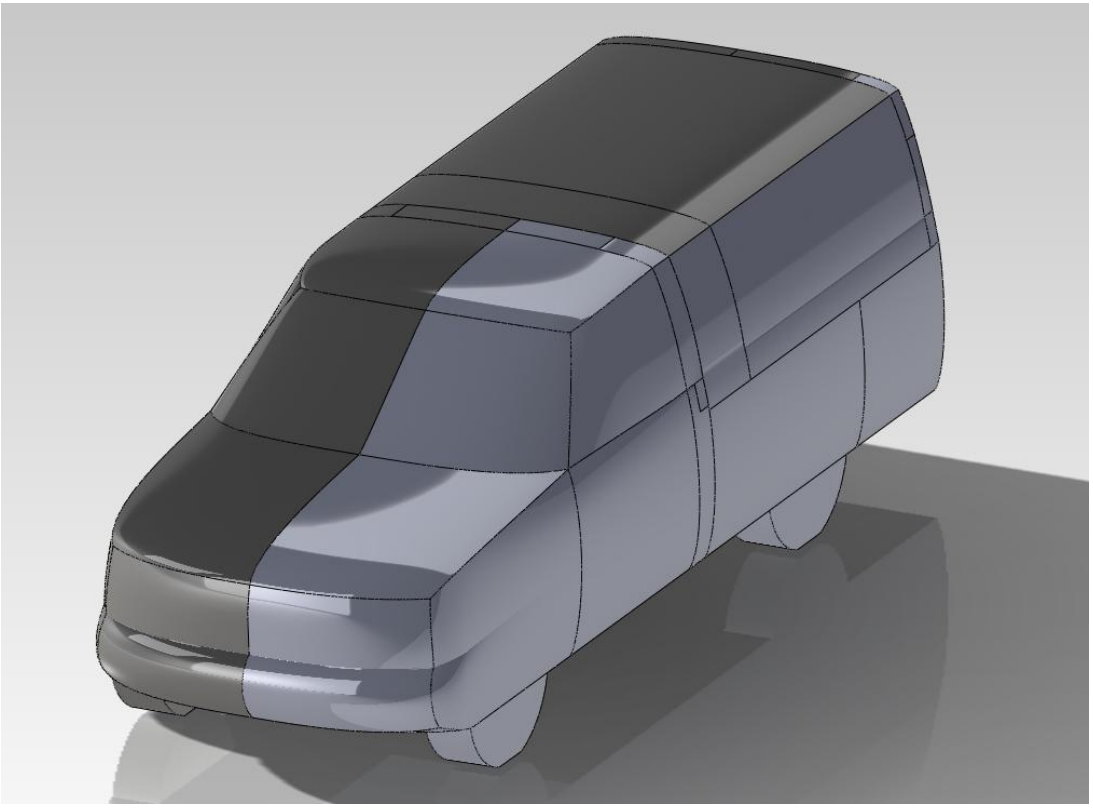

Figure 3.5 Basic SUV geometry.

3.3.2 MESH SETUP

Due to the complexity of the simulation, limited computer resources and time, the entire model was divided using the symmetry plane at Y = 0. The next step was to name the surfaces of interest for the SUV and wind tunnel in preparation for Fluent simulation. The SUV consists of a total of eight surfaces of interest, which include the following: 1) Bumper, 2) Hood, 3) Windshield, 4) Roof, 5) Rear, 6) Underbody, 7) Wheels and 8) SUV Side. The wind tunnel has a total of three surfaces of interest which include: 1) Inlet, 2) Outlet and 3) Wind Tunnel Sides. The meshing method used for the wind tunnel was the

"Patch Conforming Tetrahedron". This method is appropriate for CAD models that contain many surfaces and short edges. It reduces the amount of input necessary for mesh development, while still generating a good quality mesh. For the SUV body, a patch conforming method was used in conjunction with a five layer inflation point located throughout the top surfaces on the body due to their ability to adjust to complex bodies. The surface mesh sizing elements consisted of a minimum of *5 mm* and maximum of *15 mm* with a growth factor of 1.2.

3.3.3 FLUENT SOLVER PARAMETERS

Before the Fluent simulation can be performed it is necessary to declare the initial parameter settings. These parameter settings include defining whether the model being tested is 2D or 3D, viscous model, boundary conditions, solution control residual monitors, as well as the inlet and outlet conditions of the wind tunnel. Solver settings and conditions for the benchmark simulation can be found in ***Table 3.1***, ***Table 3.2*** and ***Table 3.3 and Table 3.4***.

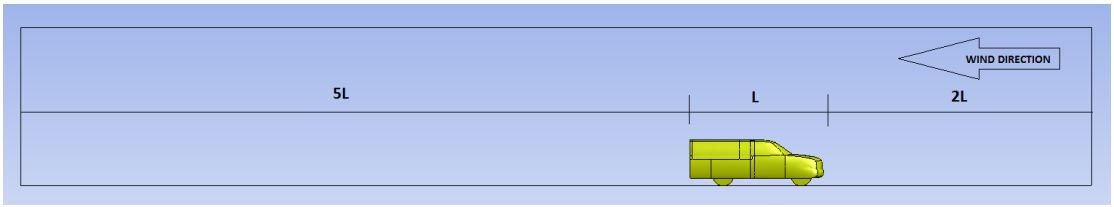

Figure 3.6 SUV orientation in relation to the wind tunnel

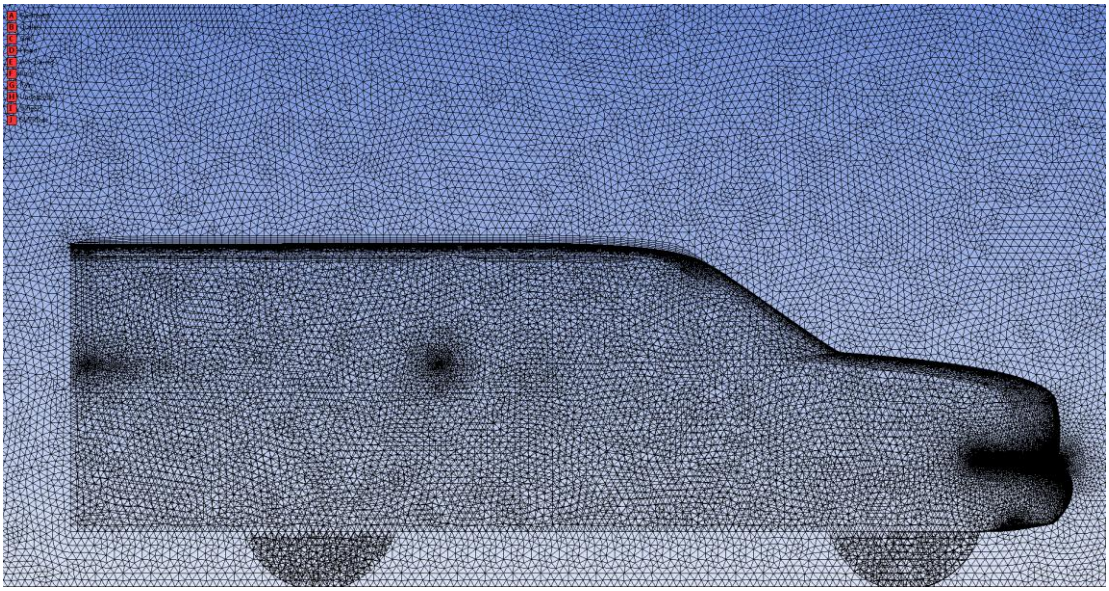

Figure 3.7 Meshing: Patch-conforming method with inflation layer on roof.

Condition	***Specification***
CFD Simulation	*3ddp (3-D Double Precision)*
Solver	
Solver	*Segregated*
Space	*3D*
Formulation	*Implicit*
Time	*Steady*
Velocity Formulation	*Absolute*
Gradient Option	*Cell-Based*
Porous Formulation	*Superficial Velocity*

Table 3.1 Solver Settings

Viscous Model	
Model	*k-epsilon (2 eqn)*
k-epsilon Model	*Standard*
Near-Wall Treatment	*Standard Wall Functions*
Operating Conditions	*Ambient*

Table 3.2 Viscous Model Settings

Boundary Conditions	
Velocity Inlet	- $30\ m/s$ *(constant)* - *Turbulence Specification Method: Intensity and Viscosity Ratio* - *Turbulence Intensity* = 1.00% - *Turbulence Viscosity Ratio* = 20 - *Normal to Boundary*
Pressure Outlet	- *Gauge Pressure Magnitude: 0 pascal* - *Backflow Direction Specification Method: Normal to Boundary* - *Turbulence Specification Method: Intensity and Viscosity Ratio* - *Backflow Turbulence Intensity* = 10% - *Backflow Turbulent Viscosity Ratio* = 10
Wall Zones	*No Slip*
Fluid Properties	- *Air* - $\rho = 1.225\ (kg/m^3)$ - $v = 4.32 \times 10^{-6}\ (kg/m \cdot s)$

Table 3.3 Boundary conditions and fluid properties

Solution Controls	
Equations	*Flow and Turbulence*
Pressure-Velocity Coupling	*Simple*
Discretization	- *Pressure: Standard* - *Momentum: Second Order Upwind* - *Turbulence Kinetic Energy: Second Order Upwind* - *Turbulence Dissipation Rate: Second Order Upwind*
Monitor	*Residuals & Drag Coefficient*
Convergence Criterion	- *Continuity = 0.001* - *X-Velocity = 0.001* - *Y-Velocity = 0.001* - *k = 0.001* - *epsilon = 0.001*

Table 3.4 Solution controls and residuals

3.3.4 RESULTS

The results of the benchmark and current simulation will now be compared to determine how well they match. The calculated Reynolds number for the benchmark as well as the simulations is 8.00×10^5, based on a velocity of $V = 30\ m/s$ and a

characteristic length of $L = 0.432\ m$. As was previously mentioned, only the C_P plots over the cab and underbody were calculated for the benchmark comparison. ***Figure 3.8*** shows the simulated C_P plots for the cab and underbody sections respectively, while ***Figure 3.9*** shows the benchmark results. Something important to note about the benchmark results shown in ***Figure 3.9*** is that the vertical axis is inverted, with negative values of C_P on the top and positive values on the bottom of the graph, as previously mentioned in *Section 3.2.3*. Taking this into account, it is evident that the simulated results closely resemble those of the benchmark. For example, the maximum C_P value from the simulation (***Figure 3.8***) is at about *1.01* and is found near the front bumper of the SUV. This closely matches the C_P value of *1.00* found in the benchmark ***Figure 3.9***. Point 9 on the benchmark graph is located at the bottom edge of the windshield and corresponds to a C_P value of *0.55*. Likewise, the graph obtained from the simulation shows a C_P value of *0.57*. Finally, moving to the top edge of the windshield, denoted by point 13 on the benchmark graph, we see a C_P value of *-0.95*, much like the results we obtained from the simulation, which is *-0.98*. Studying the curve that corresponds to the underbody, once again we can see that simulation results resemble those of the benchmark. ***Figure 3.10*** shows the velocity streamline profile for the original benchmark on the left and the simulated results on the right. From these results we can see there are two circulatory flow patterns that develop in the wake region of the models. A prominent feature of the flow is a strong upsweep between the two circulatory flow regions. The reason for this behavior is that some of the streamlines that originate from the underbody

do not stay in the bottom region, but rather cross over to the top shear layer and the top circulatory region. This shows a rapid upward acceleration of the underbody flow.

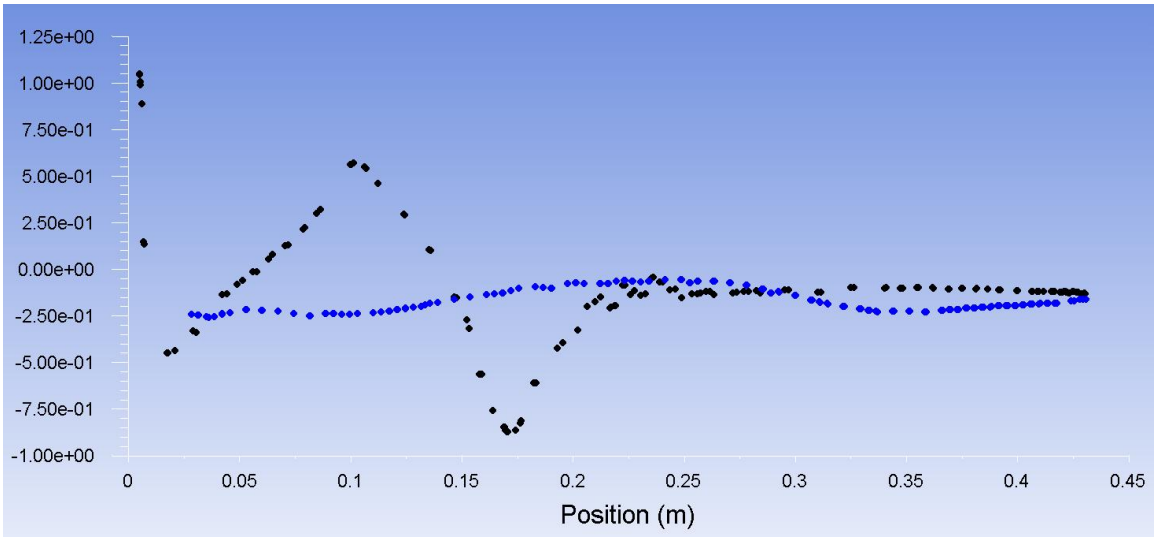

Figure 3.8 Simulated results of Cp plot over cab and underbody areas.

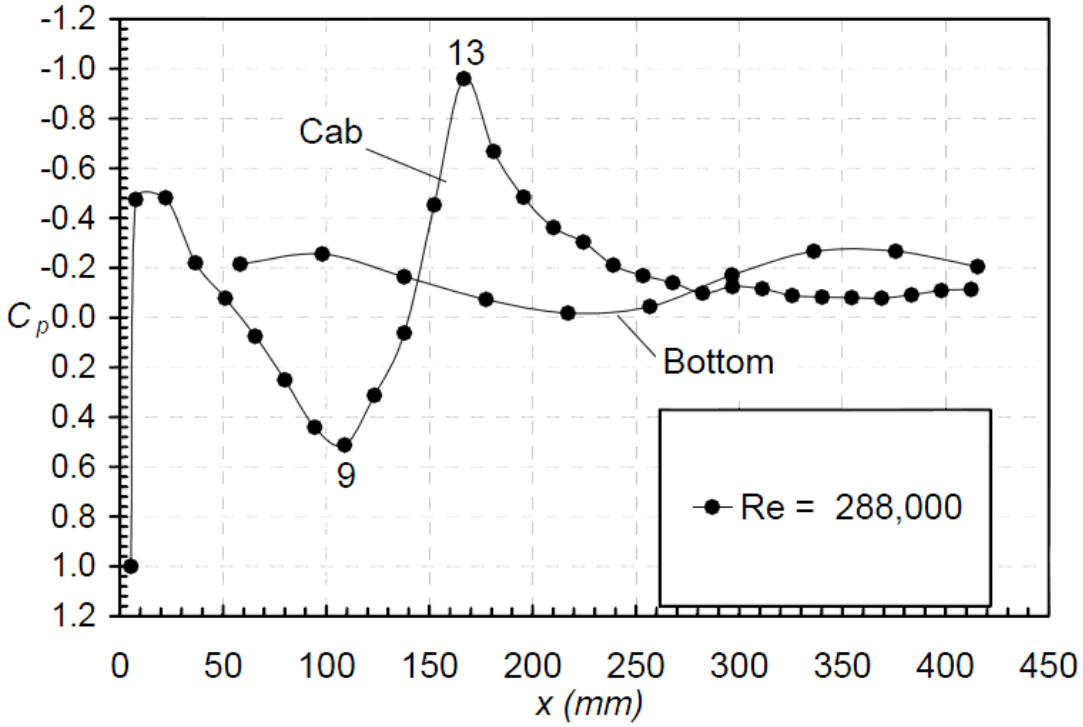

Figure 3.9 Benchmark Cp plot for the cab and bottom sections of the SUV [4].

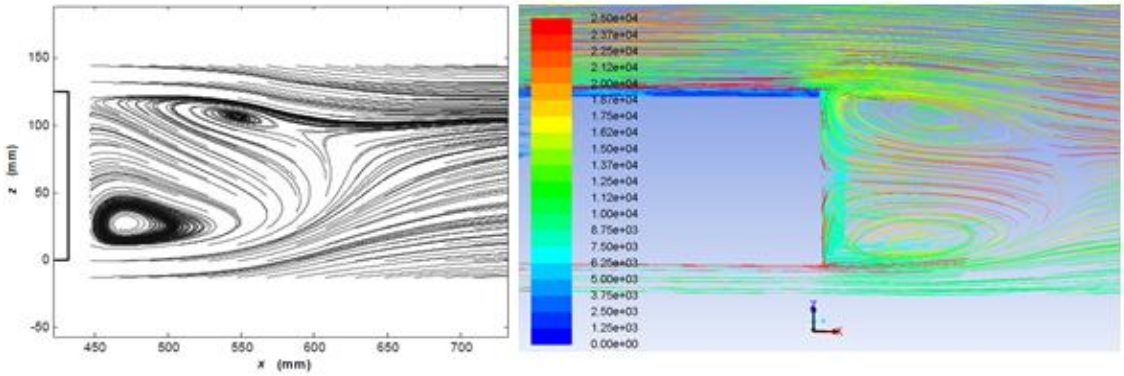

Figure 3.10 Comparison velocity magnitude streamlines [4]

3.4 CONCLUSION

From the simulation results and the setting shown above, we can conclude that the results provide a suitable turbulence model and mesh settings which can be used for the optimization process of the vortex generators (VG). The results of the simulation agree well with experimental results for downstream components considered. If the results are to be made completely reliable, additional simulations will need to be made, without using any symmetry plane. However, a complete domain simulation would require a substantial investment in additional computer resources, which is beyond the present work of this thesis.

Chapter 4

EFFECT OF VORTEX GENERATORS ON SUV MODEL

4.1 INTRODUCTION TO VORTEX GENERATORS

Vortex generators come in several shapes and sizes, which include bump-shaped VGs, delta wings, air tabs and wishbone amongst others. One of the most commonly used designs is the delta wing as seen on ***Figure 4.1***. A typical delta wing VG device has a trapezoid-shaped design that resembles a fin as seen. They are typically placed close to the rear edge of the roof, right where air flow separation is likely to occur. The benefit of using VGs is that they can potentially reduce aerodynamic drag, separation of air flow in the rear as well as reducing turbulence. This in turn can contribute to a vehicle's fuel economy, down force, top speed and velocity. In addition, the design also provides an aesthetically pleasing look, for those vehicle owners who prefer a more subtle look on their vehicles, while still benefitting from drag reduction, without having to resort to other more prominent looking aerodynamic devices, such as wings and spoilers. Finally, they are relatively inexpensive and easy to install.

Figure 4.1 Mitsubishi Evolution with VGs [6].

4.2 BUMP-SHAPED VORTEX GENERATORS ON SUV MODEL

The height for the bump-shaped VGs is set at $H = 1.67\ mm$ (1:12 scale value). The length is L = 5H and width set at W = 2H. Finally the trailing edge was cut at an angle of 27°. ***Figure 4.2*** shows the view of the bump-shaped vortex generator. The CAD model of the SUV from the benchmark was modified using Solidworks®. A total of thirteen VGs were added to the rear section of the roof on the SUV model, approximately *8.33 mm* (1:12 scale value) from the rear edge of the roof. Additionally, the VGs were spaced at *8.33 mm* (1:12 scale value) intervals. The position of the VGs is based on the

tests performed by Mitsubishi Motors. ***Figure 4.3*** shows the position of the bump-shaped VGs on the SUV model.

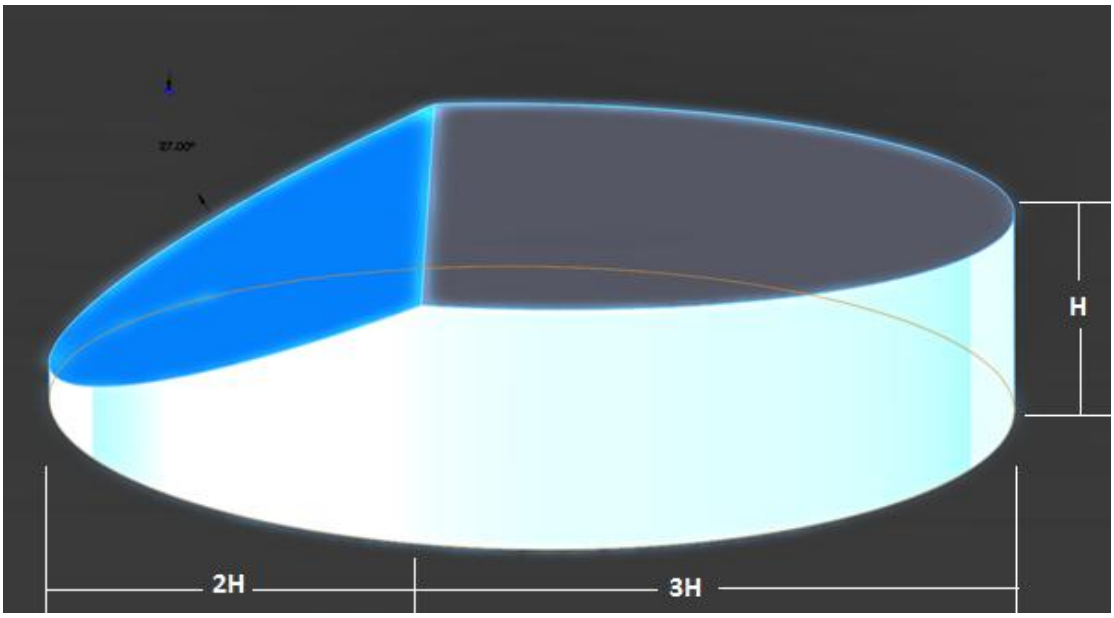

Figure 4.2 Bump-shaped VG design with dimensions.

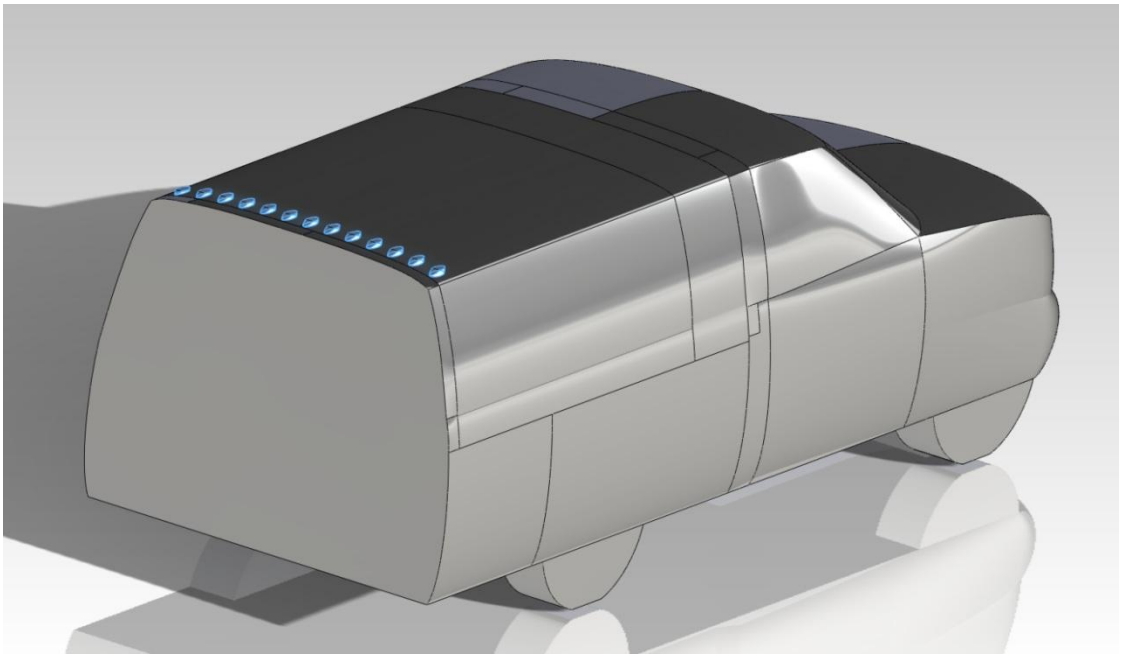

Figure 4.3 Location of bump-shaped VGs on SUV model.

4.3 DELTA WING VORTEX GENERATORS ON SUV MODEL

For the delta wing VGs the height was set at *H = 1.67 mm* (1:12 scale value). The length is L = 2H and width set at W = *0.42 mm (1:12 scale value)*. Finally the trailing edge was cut at an angle of 60°. ***Figure 4.4*** shows the view of the delta wing vortex generator. The CAD model of the SUV from the benchmark was modified using Solidworks®. A total of seventeen VGs were added to the rear section of the roof on the SUV model, approximately *8.33 mm* (1:12 scale value) from the rear edge of the roof. Additionally, the VGs were spaced at *8.33 mm* (1:12 scale value) intervals. The position of the VGs is based on the tests performed by Mitsubishi Motors. ***Figure 4.5*** shows the position of the bump-shaped VGs on the SUV model.

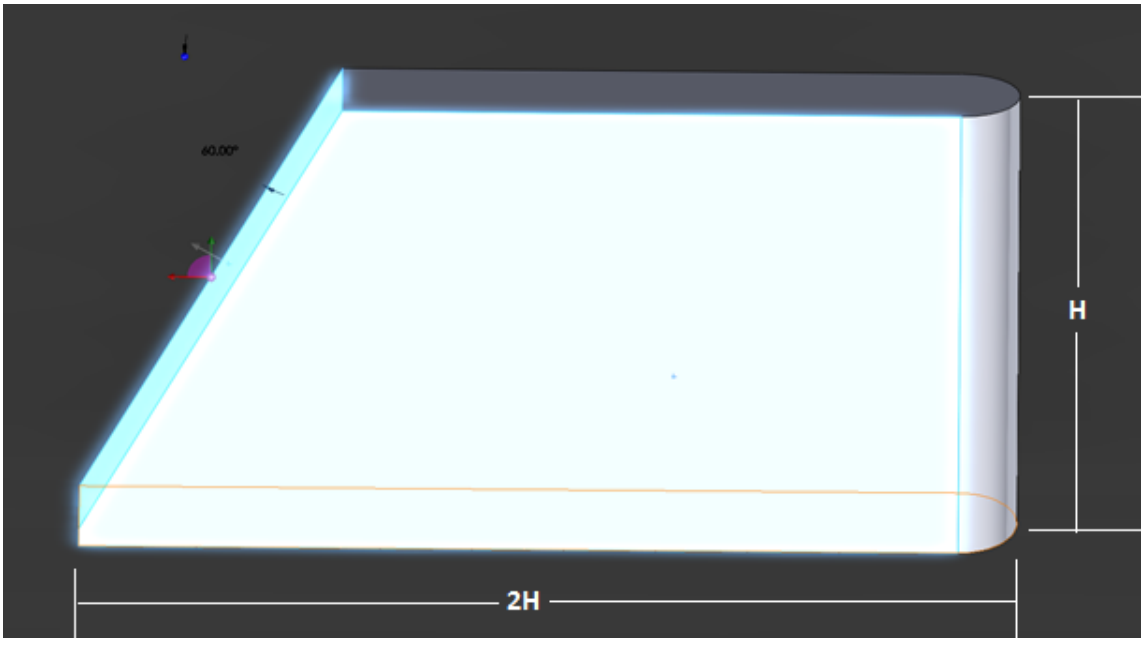

Figure 4.4 Wedge-shaped VG design

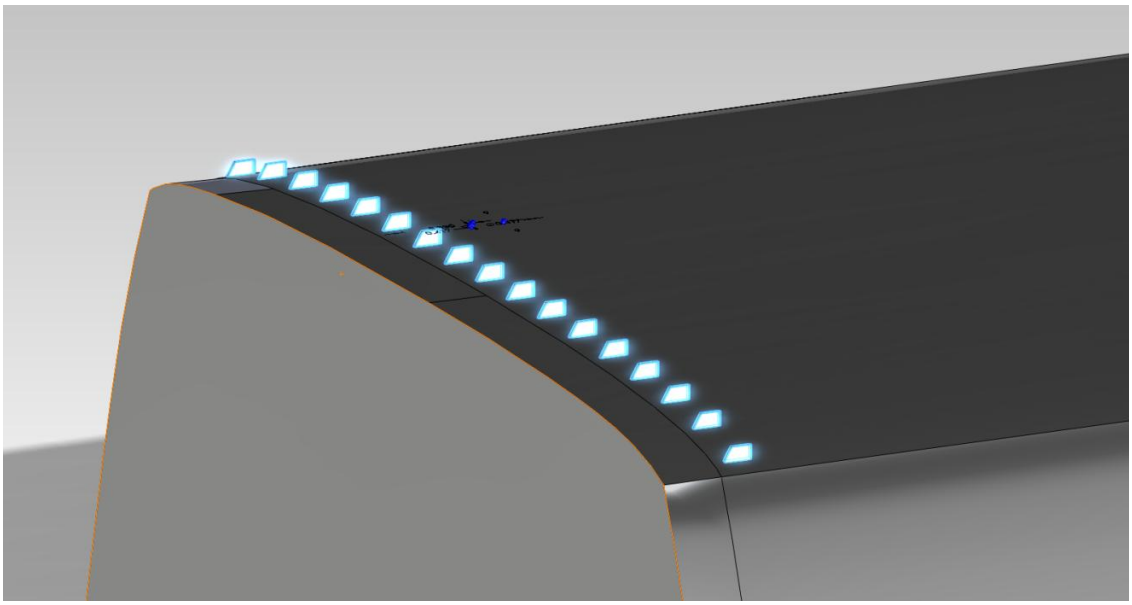

Figure 4.5 Location of wedge-shaped VGs on SUV model.

4.4 WIND TUNNEL AND VEHICLE ORIENTATION

The wind tunnel size and dimensions are adapted in the same way as used for the first benchmark simulation discussed in *Section 3.3.1*. The inlet section of the wind tunnel is set at $0.60 \times 0.50\ m^2$. The inlet of the wind tunnel is placed at two times the vehicle body length ahead of the SUV model. To satisfy the "boundary layer concept" we must select a Reynolds number greater than 10^4. Therefore, the air velocity at the inlet is set at *30 m/s,* which corresponds to a Reynolds number of $Re = 8.00 \times 10^5$. Furthermore, the outlet of the wind tunnel is placed at five times the length of the SUV model measured from the rear of the SUV model. Finally, the pressure outlet is set the atmosphere. ***The Figure 4.6*** shows a preview of the orientation of the SUV in relation to the wind tunnel.

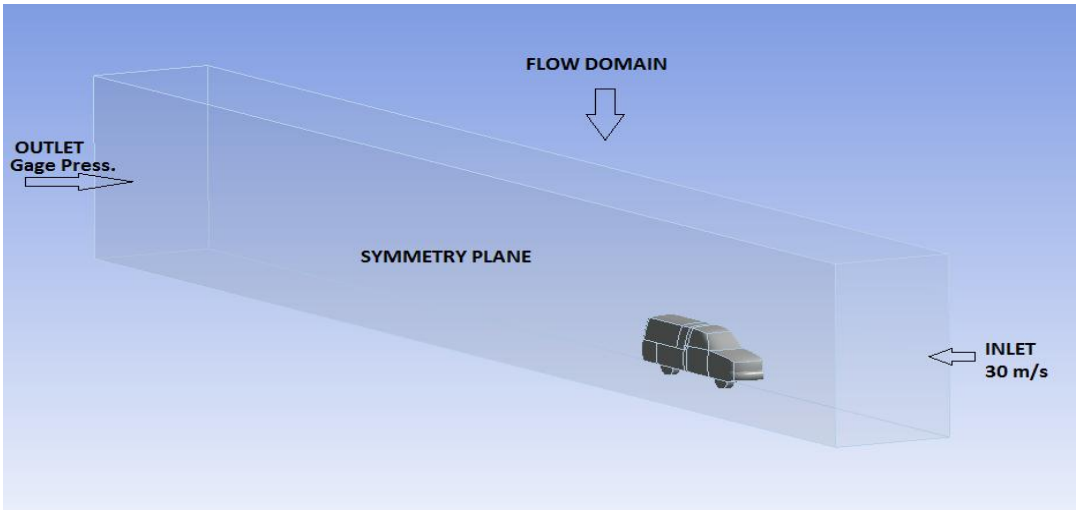

Figure 4.6 Wind tunnel and SUV orientation.

4.5 MESH AND SOLVER SETTINGS

The benchmark from Chapter 2 will be used as a reference for the mesh settings used in all the simulations performed for the vortex generators. Therefore, two patch-conforming methods are used in the simulations. Furthermore, the patch-conforming method being applied to the SUV body has a 5-layer inflation point added with a 1.2 growth factor. To verify the quality of the mesh, the skewness value was measured for each mesh. Skewness is a dimensionless value that checks for consistency and quality of a generated mesh. Additionally, the value can range between 0-1, with lower values representing better quality. It is generally recommended to keep the value below 0.95. Based on the results shown on ***Table 4.1,*** we can see that the average skewness value is *0.21*, which indicates that a good quality mesh was generated for the models. ***Figure 4.7***

and ***Figure 4.8*** show the generated mesh at the symmetry plane for the bump-shaped VG and delta wing VG respectively.

SUV MODEL	MESH METHOD	MAX. SKEWNESS	AVG. SKEWNESS
Base:	Patch-conforming	0.9591	0.2174
Bump-shaped VG:	Patch-conforming	0.8964	0.2192
Delta Wing VG:	Patch-conforming	0.8985	0.2198

Table 4.1 Mesh quality results for the SUV models.

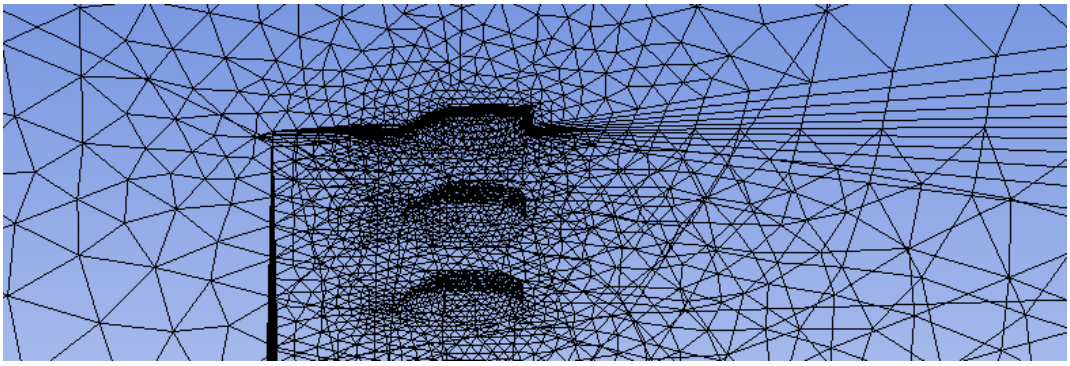

Figure 4.7 Patch-conforming meshing method near bump-shaped VGs.

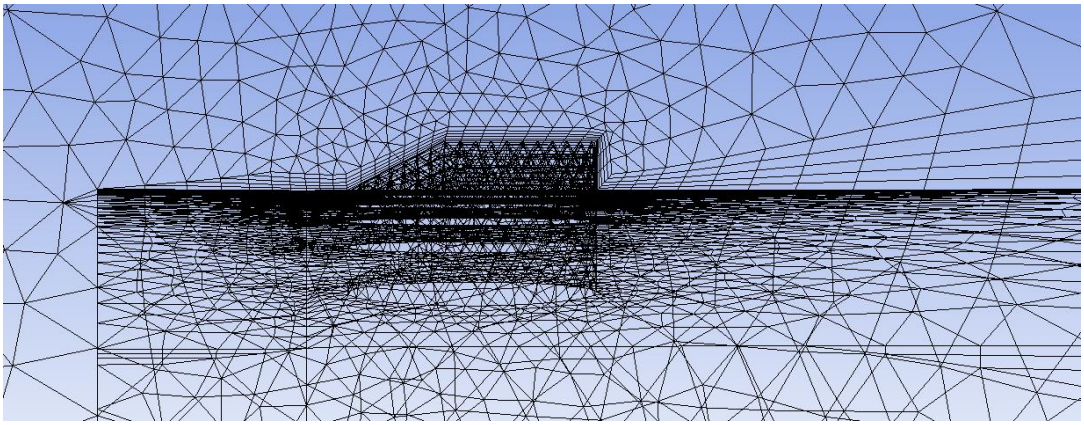

Figure 4.8 Patch-conforming meshing method near the wedge-shaped VGs.

4.6 RESULTS

4.6.1 BUMP SHAPED VS WEDGE-SHAPED VG RESULTS

Gillespie explains that the pressure gradient along the surface of a vehicle acts to push the air along the boundary layer which helps to impede its growth [2]. Therefore, pressure decreasing along the direction of flow is known as "favorable pressure gradient" because it inhibits the boundary layer growth. Vortex generators work by delaying the flow separation that occurs on the surface. Therefore, by decreasing the pressure, the velocity of the air flow should increase, which in turn will help move the separation point further down on the surface of the vehicle, effectively delaying the flow separation and thus helping to reduce drag. ***Figure 4.9*** shows the pressure contours generated in the symmetry plane by the base SUV model. We can see that the pressure contours maintain their general pattern throughout the surface of the roof. The result from the CFD simulation shows that the base SUV model generated a drag coefficient of $C_D = 0.4365$. The next model that was tested was the SUV with the bump-shaped vortex generators. Analyzing the pressure contours on the model with bump-shaped VGs in ***Figure 4.10***, we can observe that at a point upstream of the VG, the pressure contours maintain a constant pattern as that of the model with no VGs. However, as the air flow makes its way around the VGs, pressure begins to decrease, which causes the air flow velocity to increase as it makes its way pass the VGs, effectively delaying air flow detachment and decreasing drag. Results from the simulation of the model with bump-shaped VGs show a drag coefficient of $C_D = 0.4247$, which represents a decrease of *0.012*. This is a *2.7%*

improvement in drag on the SUV model. Finally, ***Figure 4.11*** shows the pressure contours from the SUV model equipped with wedge-shaped VGs. The wedge-shaped VGs also reveal a decrease in pressure, just passed the trailing edge of the VGs. This results in an increase in air flow velocity, which effectively contributes to the delay of flow separation. However, the effect is smaller than that of the bump-shaped VGs. The simulation reveals a total pressure coefficient of $C_D = 0.4263$, which represents a decrease of 0.01 from the base SUV model. This is a 2.3% improvement over the base SUV model.

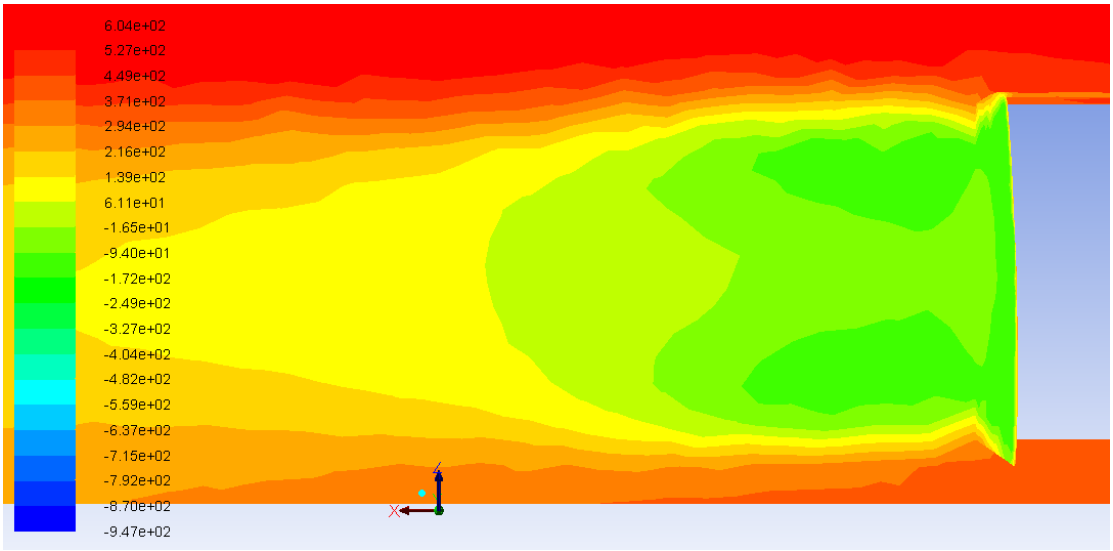

Figure 4.9 Pressure contours from SUV model with no VGs.

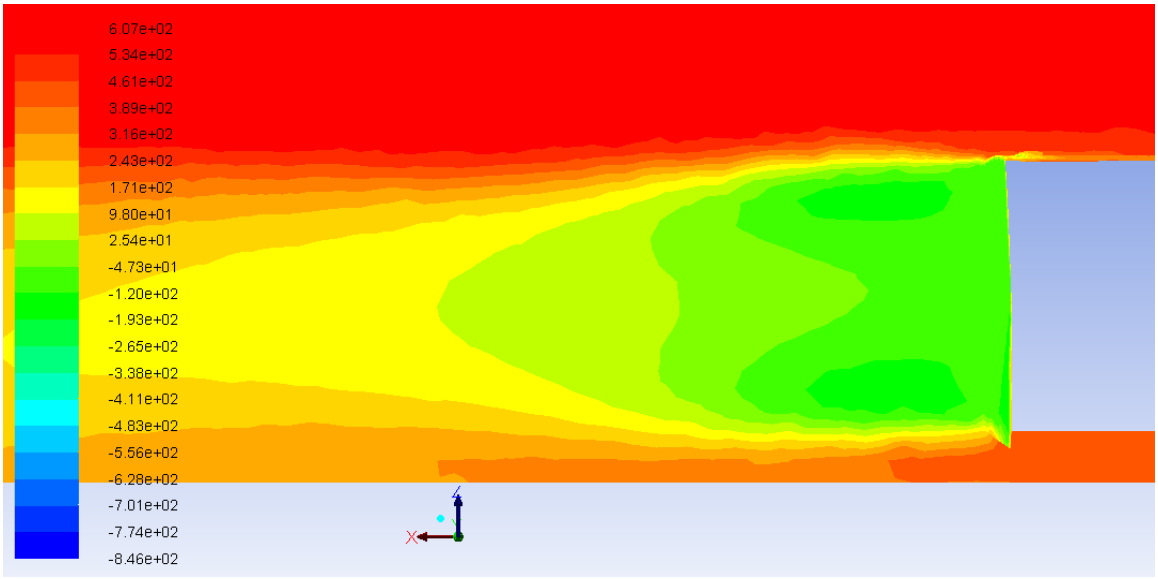

Figure 4.10 Pressure contours from SUV model with bump-shaped VGs.

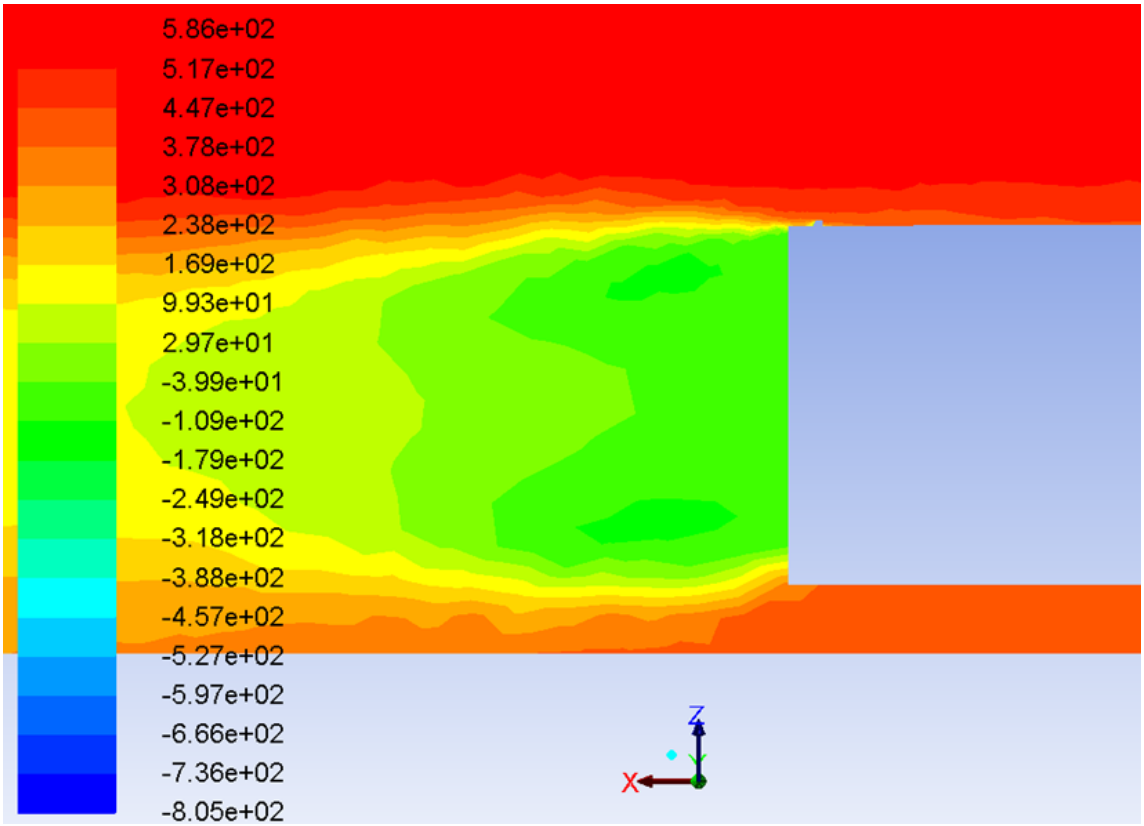

Figure 4.11 Pressure contours from SUV model with wedge-shaped VGs.

Simulation #	Modification	Cd	Difference (Cd)	% Improvement (Cd)
1	Base SUV, no VGs	0.4365	-	-
2	Bump Shape VGs	0.4247	-0.012	2.7%
3	Wedge Shape VGs	0.4263	-0.010	2.3%

Table 4.2 Drag Results from simulations.

4.6.2 EFFECT OF VG HEIGHT ON DRAG

Now that we have determined that the bump-shaped VGs provide a lower coefficient of drag C_D, the next step is to determine the proper height for the VGs used on the SUV model. Typically the best results are obtained when the VG height is close to that of the boundary layer thickness. As was previously noted by Koike, Nagayoshi and Hamamoto, VGs with a height between *20 mm* and *25 mm* typically yield the best results. Five different heights were tested to determine which one provides the lowest coefficient of drag. The values tested were *H = 15 mm, 20 mm, 25 mm, 30 mm and 40 mm.* Taking a look at the pressure contours near the wake region for the varying VG heights, it's possible to observe some differences between them as the height of the VG increases as see on ***Figure 4.12***. Starting with the top two contour shapes, corresponding the base model with no VGs on and the adjacent on showing VGs with a height *H = 15 mm* respectively. We can observe generally broad bell-shaped contours for both models. The base model yielded a $C_D = 0.4365$, while the *15 mm* VG resulted in a $C_D = 0.4226$. Moving on to the two middle contour shapes in ***Figure 4.12***, we start to see more

streamlined and elongated pressure contours. The two middle contour shapes correspond to a VG height of *20 mm* and *25 mm* respectively. This two models produced pressure coefficients of $C_D = 0.4248$ and $C_D = 0.4215$ respectively. Finally, we turn to the bottom two pressure contour shapes in ***Figure 4.12***, which correspond to a VG height of *30 mm* and *40 mm* respectively. We notice that the contours appear broader than the ones in the middle, which indicates that the wake region is once again getting bigger, with a resemblance to top ones. The coefficient of drag for the bottom two pressure contours were $C_D = 0.4232$ and $C_D = 0.4333$ respectively. Based on the results obtained from the simulations, the VG that yields the lowest coefficient of drag C_D is the one with a height of $H = 25\ mm$. This seems to agree with the observations made by Koike, Nagayoshi and Hamamoto. This indicates that for the SUV model, VGs with a height $H = 25\ mm$ are closest to the boundary layer thickness and thus yield the best results. ***Figure 4.15*** shows a plot of the results for difference VG heights.

Figure 4.13 and ***Figure 4.14*** offer a closer look at the flow behavior as they move around the VGs.

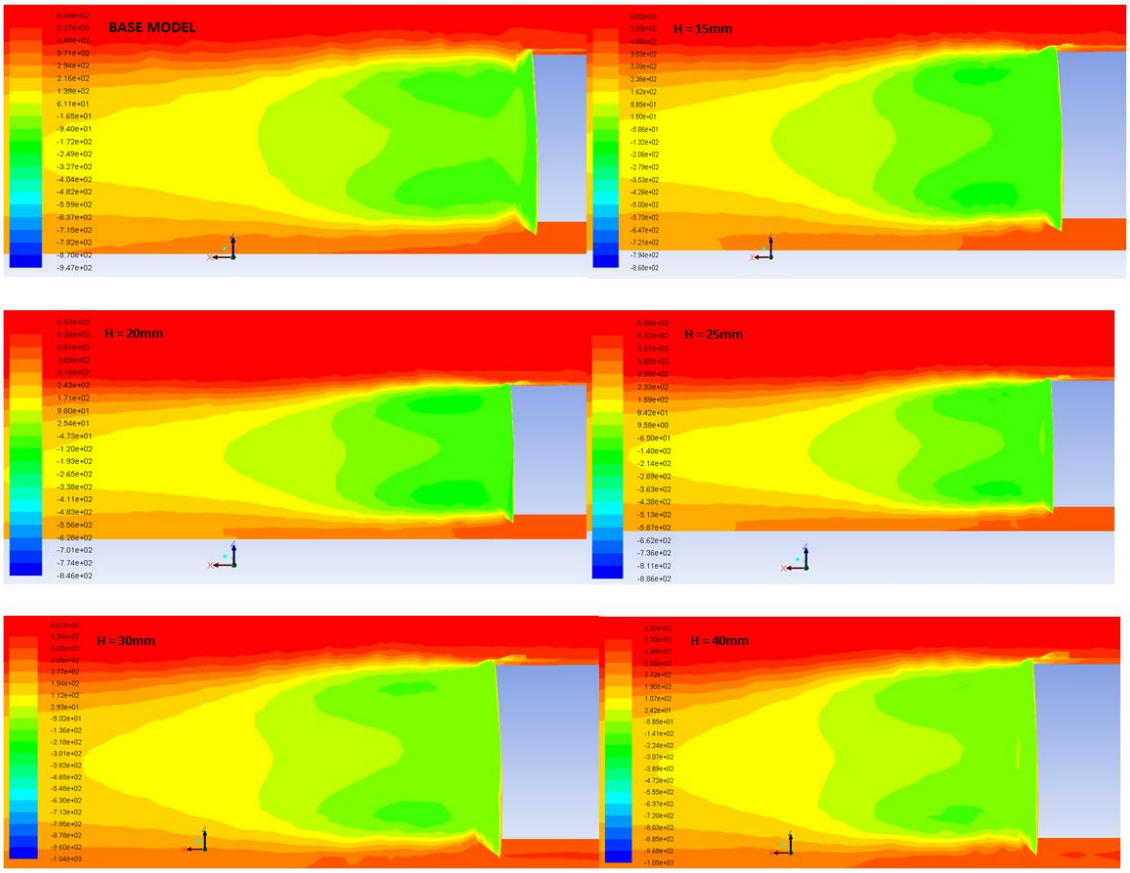

Figure 4.12 Pressure contours in wake region for varying VG heights.

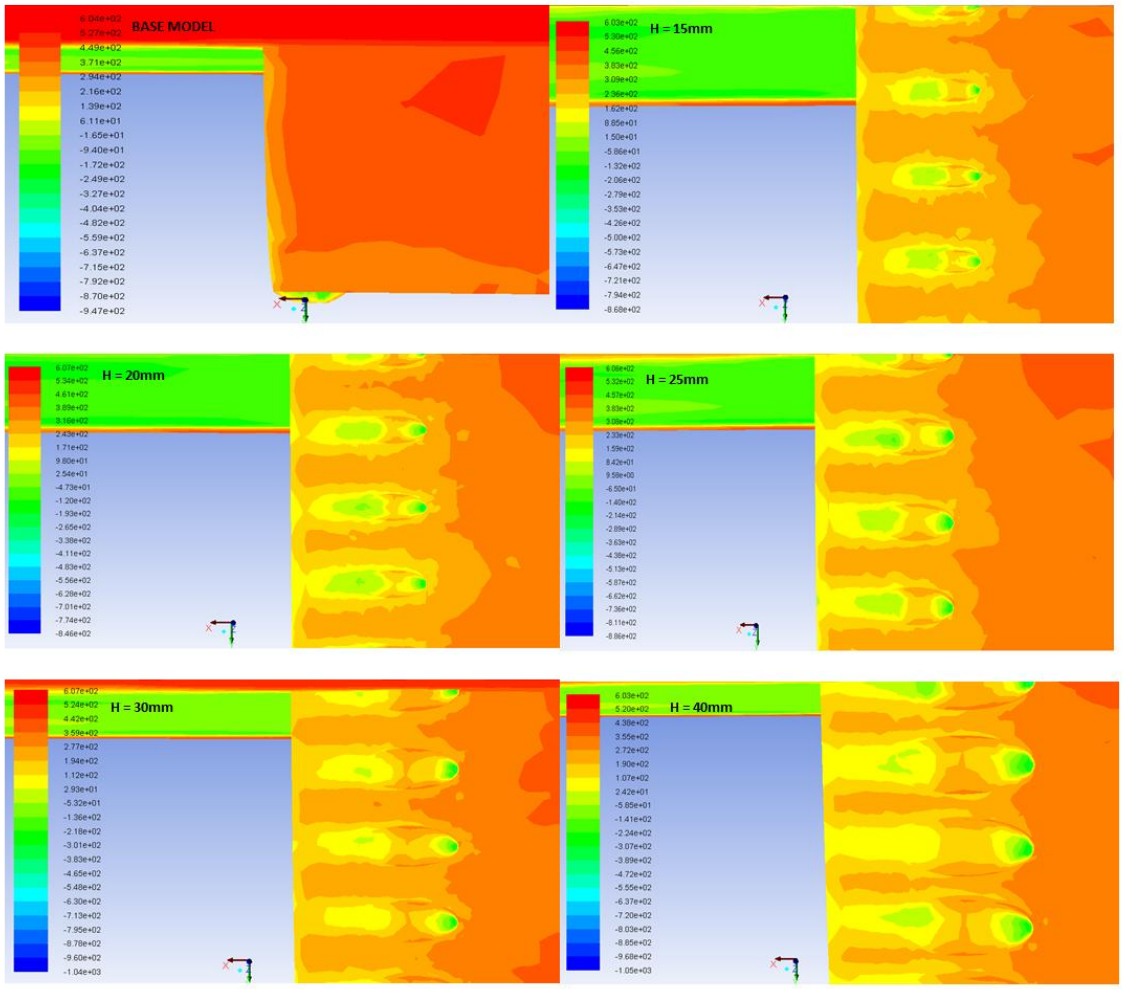

Figure 4.13 Pressure contours on roof of SUV for varying VG heights.

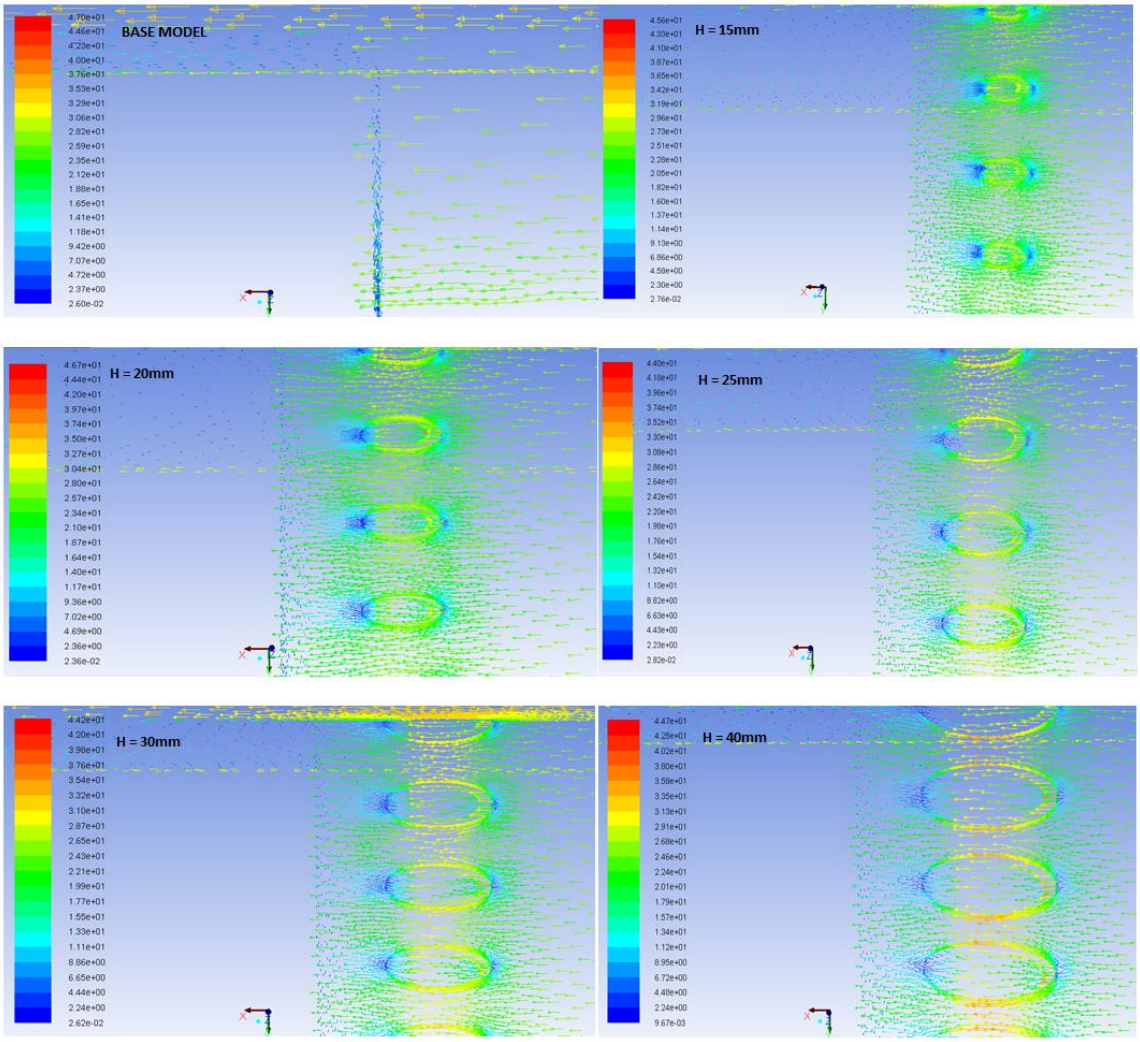

Figure 4.14 Velocity vectors on roof for varying VG heights.

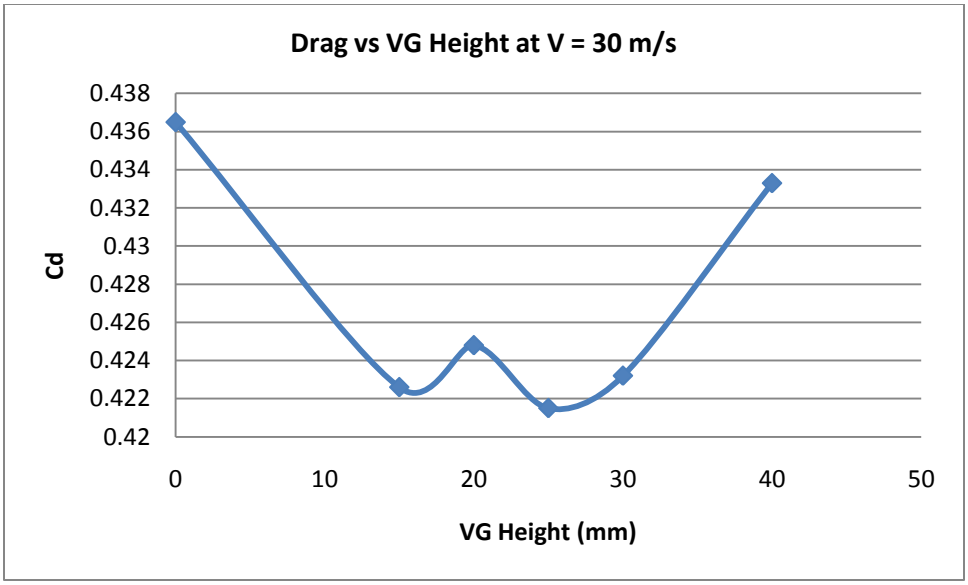

Figure 4.15 C_D for different VG heights.

4.6.3 EFFECT OF REYNOLDS NUMBER ON DRAG

According to Hucho, the Reynolds Number is a dimensionless parameter which is a function of the speed of the vehicle V_∞, the kinematic viscosity ν of the fluid and characteristic length *l* as defined by ***Figure 4.16***. For different Reynolds numbers entirely different flows may occur for the same body geometry [1].

The formula for the Reynolds number, as it relates to the boundary layer, is as follows;

$$Re_l = \frac{V_\infty\, l}{\upsilon} > 10^4 \qquad (4.1)$$

Figure 4.17, Figure 4.18 and ***Figure 4.19*** show the results of the simulations for velocity *V = 30 m/s and V = 50 m/s*. Using V = 30 m/s, the corresponding Reynolds number is *Re*

$= 7.98 \times 10^5$ and when $V = 50$ m/s, $Re = 1.33 \times 10^6$. At $V = 30$ m/s the coefficient of drag C_D was found to be $C_D = 0.4215$ and at $V = 50$ m/s, $C_D = 0.4116$. This represents a *2.3 %* drop in C_D between the two velocity values. Preliminary results suggest that the VGs may be more effective at higher velocity values.

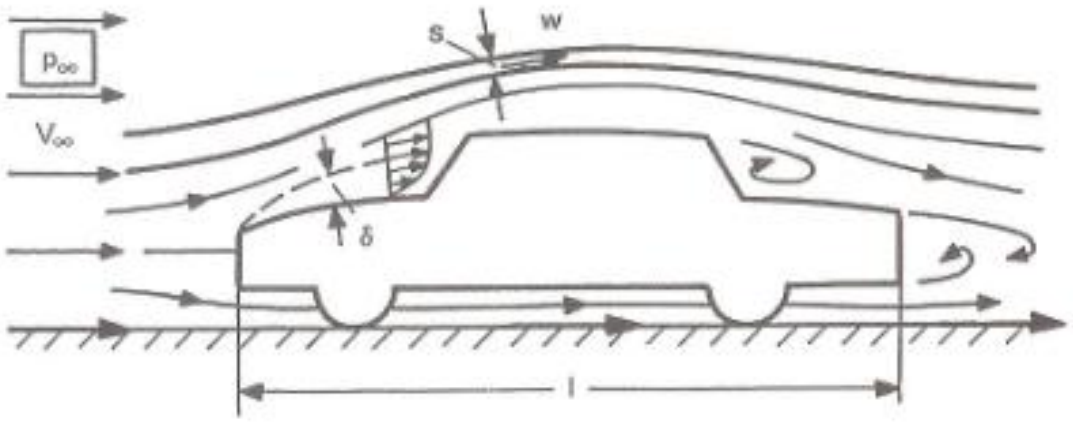

Figure 4.16 Flow around a vehicle [1].

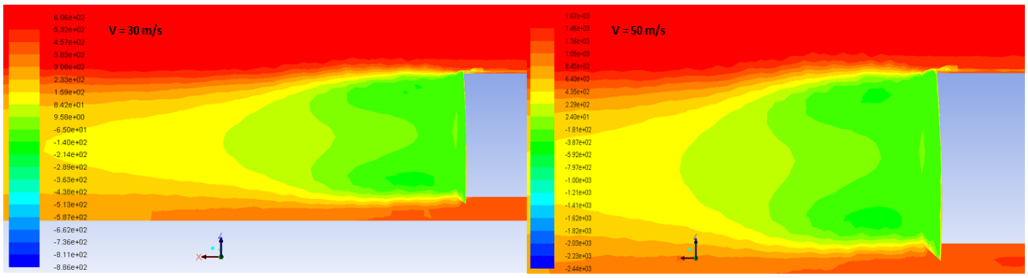

Figure 4.17 Pressure contours in wake region at different velocities.

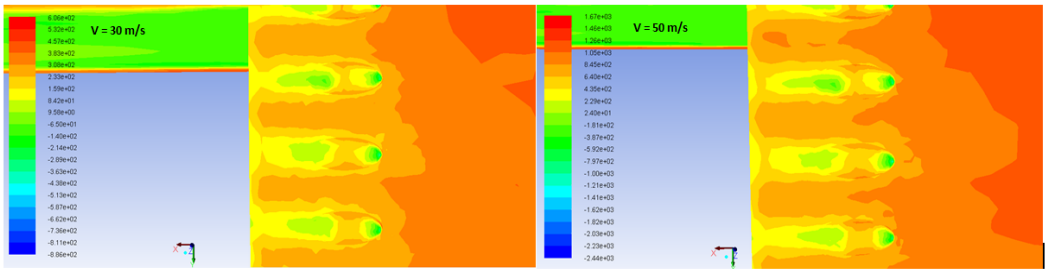

Figure 4.18 Pressure contours on roof of SUV at different velocities.

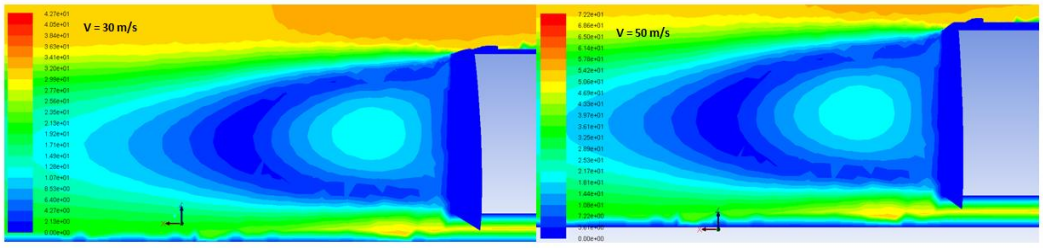

Figure 4.19 Velocity magnitude in wake region at different velocities.

Chapter 5

CONCLUSION AND FUTURE WORK

5.1 SUMMARY

This thesis started by reproducing the experimental results of the Generic SUV model by Bahram Khalighi [4] using CFD techniques. After validating the CFD setup and mesh settings, the results obtained along with the original SUV CAD model were then used to install the vortex generators. A total of three basic configurations were tested. A base SUV model containing no drag reducing devices, a second SUV model with bump-shaped vortex generators and finally a third model with the wedge-shaped vortex generator. Once it was determined that the bump-shaped VGs produced the lowest CD, when compared to the wedge-shaped VGs, the next step was to experiment with different VG heights to determine the one that was best suited for the SUV model. By analyzing the total pressure contours in the rear section of the SUV roof, we found that adding vortex generators lead to a pressure decrease in the vicinity of the VGs. In keeping with Bernoulli's equation, the resulting decrease in pressure simultaneously leads to an increase in air velocity on the surface of the SUV, which effectively helps to delay the airflow detachment by shifting the separation point further back. By moving the separation point of the boundary layer further back on the surface of the SUV, the drag coefficient C_D is reduced. It was found that bump-shaped VGs with a height of $H = 25\ mm$ were more effective than wedge-shaped VGs and resulted in a coefficient of drag of $C_D = 0.4215$. Bump-shaped VGs showed an improvement in drag reduction of 2.7%

over the base SUV model, while the wedge-shaped VGs resulted in a 2.3% improvement in drag over the base SUV model.

5.2 FUTURE WORK

Although maximum reduction of aerodynamic drag coefficient (C_D) was achieved by using bump-shaped vortex generators in the present study, further improvements to the design of the VGs needs to be made which could potentially lead to a greater reduction in the drag coefficient. Further improvements can also be made to the SUV model. For example, the model that was used for the simulations had a very simple, flat rear section and it was also missing the side mirrors. Additionally, the flow over the SUV model in the present CFD simulation was simplified due to hardware limitations. Steady flow of air with zero degree yaw angle was assumed, even though in real world applications the flow over a vehicle is unsteady and quite turbulent. The next step would be to conduct simulations in a wind tunnel facility, using a more realistic SUV model along with the optimized vortex generators incorporated into the SUV.

REFERENCES

1. Wolf-Heinrich Hucho, “Aerodynamics of Road Vehicles”, SAE International, Warrendale, PA, 1998.
2. Gillespie, T. “Fundamentals of Vehicle Dynamics”, Society of Automotive Engineers, Inc., 1992.
3. Jeff Howell and Adrian Gaylard , **“**IMPROVING SUV AERODYNAMICS **”**
4. Abdullah M. Al-Garni, Luis P. Bernal and Bahram Khalighi, “Experimental Investigation of the Flow Around a Generic SUV” SAE SAE2004-01-0228.
5. Masaru Koike, Tsunehisa Nagayoshi and Naoki Hamamoto, “Research on Aerodynamic Drag Reduction by Vortex Generator”, Mitsubishi Motors Technical Reviews, 2004.
6. Andrew L. Heyes, David A.R. Smith, “Modification of a Wing Tip Vortex by Vortex Generators”, Elsevier, 23 May 2005, ScienceDirect.
7. Azize Akcayolu, “Flow Past Confined Delta-Wing Type Vortex Generators”, Elsevier, 19 August 2010, ScienceDirect.
8. Frank K. Lu, Qin Li, Chaoqun Liu, “Micro Vortex Generators in High-Speed Flow”, Elsevier, 2010, ScienceDirect.
9. A. Lemouedda, M. Breuer, E. Franz, T. Botsch, A. Delgado, “Optimization of the Angle of Attack of Delta-Winglet Vortex Generators”, Elsevier, 4 August 2010, ScienceDirect.

10. C. Ramesh Kumar, “Study of Aerodynamic Drag Reduction using Vortex Generators”, International Journal of Advanced Engineering Sciences and Technologies, Vol. No. 10, Issue No. 1, 181-183, 2011.
11. Torbjorn Gustavsson, Tomas Melin, “Application of Vortex Generators to a Blunt Body”, KTH Engineering Sciences, Department of Aeronautical and Vehicle Engineering, Royal Institute of Technology, 2006.
12. Hua Shan, Li Jiang, Chaoqun Liu , Michael Love and Brant Maines, “Numerical study of passive and active flow separation control over a NACA0012 airfoil”, Elsevier, 10. December 2007, ScienceDirect.
13. NASA :: Website "Micro-Vortex generators enhance Aircraft Performance", http://www.nasa.gov/centers/langley/news/factsheets/Micro-VG.html
14. Streamlines image :: Website: http://autospeed.com/cms/title_Aero-Testing-Part-4/A_108676/article.html
15. C. H. K. Williamson, “Three Dimensional Vortex Dynamics in Bluff Body Wakes”.
16. U.S. Department of Energy, Energy Efficiency and Renewable Energy, http://www.fueleconomy.gov/feg/atv.shtml
17. Mathieu Roume´as, Patrick Gillie´ron, and Azeddine Kourta, “Analysis and control of the near-wake flow over a square-back geometry”.
18. Vortex Generator image :: Website : http://mbworld.org/forums/attachments/e-class-w124/136327d1217550876-possible-modifications-1991-300ce-evobumps.jpg